İZMIR KATİP ÇELEBİ UNIVERSITY
GRADUATE SCHOOL OF NATURAL AND APPLIED SCIENCES

INVESTIGATION OF GOLD NANOPARTICLE DOPING ON THE SENSING PROPERTIES OF POLYPYROLE BASED CONDUCTING POLYMER

M.Sc. THESIS

Abdullah BAYRAM

Material Science and Engineering Programme

Thesis Advisor: Prof.Dr.Salih OKUR

JANUARY 2014

İZMİR KATİP ÇELEBİ UNIVERSITY
GRADUATE SCHOOL OF NATURAL AND APPLIED SCIENCES

INVESTIGATION OF GOLD NANOPARTICLE DOPING ON THE SENSING PROPERTIES OF POLYPYROLE BASED CONDUCTING POLYMER

M.Sc. THESIS

Abdullah BAYRAM
(Y120111003)

Department of Material Science and Engineering

Thesis Advisor: Prof. Dr. Salih OKUR

JANUARY 2014

Abdullah Bayram, a **M.Sc.** student of **İzmir Katip Çelebi University** student ID Y20111003, successfully defended the **thesis** entitled "**Investıgatıon of gold nanopartıcle doping on the sensing propertıes of polypyrole based conducting polymer**", which he prepared after fulfilling the requirements specified in the associated legislations, before the jury whose signatures are below.

Thesis Advisor:	**Prof. Dr. Salih OKUR** İzmir Katip Çelebi University	.....
Jury Members:	**Doç. Dr. Şerafettin DEMİÇ** İzmir Katip Çelebi University	.....
	Yard. Doç. Dr. Ömer MERMER Ege University	.....

Date of Submission: 30 December 2013
Date of Defense : 10 January 2014

To my family,

ACKNOWLEDGEMENT

I would especially like to thank my advisor, Professor Salih Okur, for his healthy degree of optimisms. I would also like to thank Dr. Hamida Darwish in Kingdom of Saudi Arabia for garnered me in her group; they encouraged sharing of ideas, insightful discussions and a productive work environment.

Next, I would like to thank to Dr. Mehmet Şenel who synthesized polymers and polymer composites that I have used in my thesis. I am also thankful to Dr. Mustafa Can for his directive advices for my entire thesis especially at result and discussion part.

Next, I would like to thank my group members who encouraged me to continue to work hard when motivation was low, provided advice when I was stumped and lost, delivered comic relief when it was sorely needed and reminded me the important things in life when I forgot. I would also like to thank my lab mates Cebrail Özbek, Abdurrahman Halis Güzelaydın, Cem Baytöre and Melike Karakaya.

Without great friends and family, this endeavor would have concluded before it began. I would like to thank them for believing in me, encouraging me to continue going, and providing distractions from work when they were needed.

I want to thank my parents. It is with their help for all my life that I became who I am today. Thanks for always being there for me, believing in me and motivating me to set out on my own path. I cannot begin to describe how lucky I feel for having them as my parents. All opportunities and accomplishments I owe to them.

This Thesis was supported by the KASCT strategic technologies program in the Kingdom of Saudi Arabia – Project No. (10-NAN1407-03) and University of King Abdulaziz University, Jeddah, Saudi Arabia.

January 2014 Abdullah BAYRAM

TABLE OF CONTENTS

Page

ABBREVIATIONS

CO	**:** Carbonmonoxide
CO_2	**:** Carbon dioxide
O_2	**:** Oxygen
NH_3	**:** Ammonia
QCM	**:** Quartz crystal microbalance
HOMO	**:** Highest occupied molecular orbital
LUMO	**:** Lowest unoccupied molecular orbital
VB	**:** Valance band
CB	**:** Conduction band
IDE	**:** Interdigitated electrode
FET	**:** Field effect transistor
SAW	**:** Surface acoustic wave
$BaTiO_3$	**:** Barium titanate
PZT	**:** Lead zirconate titanate
SiO_2	**:** Silicon dioxide
MHz	**:** Megahertz
PPM	**:** Per part million
DMF	**:** Dimethylformamide
UV	**:** Ultraviolet
SCCM	**:** Standard Cubic Centimeters per Minute
PPy	**:** Polypyrrole
Fc	**:** Ferrocene
PPy-Au	**:** Polypyrrole Gold nanocomposite
PPy-Fc	**:** Polypyrrole Ferrocene nanocomposite
PPy-Au-Fc	**:** Polypyrrole Gold Ferrocene nanocomposite
GCF	**:** Gas correction factor
RPM	**:** Round per minute
HCI	**:** Hydrogen chloride
HNO_3	**:** Nitric acid
$FeCI_3$	**:** Iron (III) chloride
AC	**:** Alternating current

LIST OF TABLES

Page

LIST OF FIGURES

Page

INVESTIGATION OF THE EFFECTS OF GOLD NANOPARTICLE DOPING ON THE SENSING PROPERTIES OF POLYPYROLE BASED CONDUCTING POLYMERS

SUMMARY

Besides human health, toxic gases are harmful for both animal and plant health. Various concentrations cause so many fatal or permanent problems. Therefore, controlling toxic gases (carbon monoxide, carbon dioxide, ammonia), and oxygen at the indoor environment is of vital importance. In this study, effect of gold nanoparticle doping on the gas sensing properties of pyrrole-based conductive polymers were investigated via acoustic wave and electrical based techniques. In this study, quartz crystal microbalance technique was used. Quartz Crystal Microbalance is a powerful technique for nano scale determination of the sorption properties of materials. According to Sauerbrey relation, the mass change on quartz crystal electrode cause a certain shift in the resonant frequency of a vibrating crystal oscillator. This shift can be monitored using QCM method.

Being easily supplemented, synthesized, modified with different kinds of functional groups and improved gas sorption properties, conducting polymers are suitable for gas sensors. Polypyrrole, polypyrrole-ferrocene, polypyrrole-gold-ferrocene and polypyrrole-gold were synthesized except ferrocene and used along with pure ferrocene throughout this study. A series containing polypyrrole-based materials doped with gold nanoparticles were formed.

Dispersions containing 0.1 g of each material in 20 mL dimethylformamide (DMF) were prepared and agitated for 1 h on magnetic stirrer. The dispersions were filtered out using zero – 450 nm mesh filters. 5 μL from each of these dispersions were then drop-cast onto AT-cut gold-coated quartz crystal microbalance (QCM) electrodes. To yield higher conductance values, the prepared dispersions were directly drop-cast onto gold interdigitated (IDE) glass electrodes with 3 μm interdigit spacing without filtering. The coated electrodes were dried on hot plate at 50 °C for 1 h to deposit thin-films. The thin-film coated electrodes were placed in an electromagnetically shielded test cell specifically designed for gas measurements. An array of computer controlled mass flow meters were used to maintain CO, CO2, O2 and NH3 gas flow into the test cell with alternately varying concentration levels ranging between 0 vol% to 100 vol% in predetermined intervals. Gas sensor responses of the thin-film coated QCM electrodes were assessed by measuring the frequency shift of the vibrating quartz crystal from its natural resonance frequency due to gas sorption onto the deposited thin-films. The frequency shift are evaluated according to value into adsorbed mass consistent with Sauerbrey relation. Responses from the interdigitated electrodes were assessed by measuring the resistance changes through the thin-film coating under a compliance current value of 1.0000 mA.

Effect of gold nanoparticle doping on the gas sensing properties of pyrrole-based conductive polymers were investigated via quartz crystal microbalance and interdigitated electrode techniques. A sequence were created from PPy, Fc, PPy-Fc, PPy-Au and PPy-Fc-Au.

Modification of PPy with ferrocene caused the sensitivity of the PPy-Fc material fell down with respect to bare PPy but increased with respect to bare Fc. After gold doping to PPy-Fc the sensitivity to CO_2 increased with respect to PPy-Fc. Gold doping to PPy-Fc increased sensitivity to CO_2, whereas gold doping to PPy decreased sensitivity to CO_2 with respect to bare PPy.

Modification of PPy with ferrocene, the sensitivity of the PPy-Fc material were increased, even though bare Fc showed low sensitivity value for NH_3 gas. After gold doping to PPy-Fc the sensitivity to O_2 was higher than bare PPy, Fc and PPy-Fc, but the sensitivity to NH_3 decreased with respect to PPy-Fc giving sensitivity values close to bare PPy, whereas gold doping to bare PPy increased the sensitivity to O2 with respect to Fc and nearly was dropped to halve of the sensitivity to NH_3. From the results show that PPy, PPy-Au, Fc, PPy-Fc are selective to NH_3 with respect to the other gasses.

ALTIN NANOPARÇACIK KATKILAMANIN POLİPİROL TABANLI İLETKEN POLİMERLERİN GAZ ALGILAMA ÖZELLİKLERİNE OLAN ETKİSİNİN İNCELENMESİ

ÖZET

Toksik gazlar insan sağlığının yanında hem hayvanların hem de bitkilerin sağlığı için zararlıdır. Farklı konsantrasyonlar sağlık üzerinde çeşitli kalıcı veya ölümcül problemlere yol açarlar. Bu yüzden ortamdaki toksik gazların (karbon monoksit, karbon dioksit, amonyak) ve oksijenin ortamdaki kontrolü hayati önem arz etmektedir. Bu çalışmada, altın nanoparçacık katkılamanın pirol tabanlı iletken polimerlerin gaz algılama özelliklerine olan etkisi akustik dalga tekniği ve elektriksel ölçüm yöntemleriyle incelenmiştir. Bu çalışmada, kuartz kristal mikrobalans metodu kullanılmıştır. Kuartz kristal mikrobalans, nanogram mertebesinde, malzemelerin gaz tutma özelliklerini inceleyebileceğimiz bir tekniktir. Sauerbrey ilişkisine göre, kristal elektrotundaki kütle değişimi, titreşen kristal elektrotta belirli bir frekans kaymasına neden olur. Bu değişim QCM metodu ile ölçülebilir.

İletken polimerlerin kolayca katkılanabilmesi ve sentezinin kolay olması ayrıca kolayca farklı fonksiyonel grupların bağanabilmesi ile gaz adsorplama özellikleri iyileştirilebilir olması gaz sensor uygulamaları için uygun malzemelerdir. Bu çalışmada, polipirol temelli olarak sentezlenmiş ve altın nanokatkılanmış olan malzemelerden seri oluşturulmuştur. Polipirol, polipirol-ferrosen, polipirol-altın-ferrosen, polipirol-altın ve ferrosen çalışmada kullanılmıştır. Herbir malzemenin 10 miligramı 20 mililitre dimethylformamide (DMF) içinde dispersiyonları hazırlanmıştır. Bu dispersiyonlar manyetik karıştırıcıda bir saat karıştırılmış ve filtre aralığı maksimum 450 nanometre olan filter ile süzülmüştür

Herbir malzemenin dispersiyonu 50 mikrolitre A-T kesim kuartz kristal elektroduna damlatma ile kaplama metodu ile kaplanmıştır.Daha iyi iletkenlik alabilmek için 3 mikrometre aralıklı taraklı altın elektrotlar üzerine malzemeler filtre edilmeden damlatılmıştır. Oluşturulmuş olan filmler sıcak tabaka üzerinde 50 ^{0}C bir saat süre ile kurutulmuştur. İnce film kaplı elektrotlar, gaz ölçümlerinin yapılabilmesi için tasarlanmış, elektromanyetik alan korumalı test hücresi içine yerleştirilmiştir. Bilgisayar kontrollü kütle akışmetreler ile önceden belirlenen zaman aralıklarında hacmen %0 ve %100 arasında değişebilen konsantrasyonlarda, ortama CO, CO_2, O_2 ve NH_3 gazları gönderilmiştir.Gönderilen gazın QCM electrodundaki film yüzeyine adsorbe veya absorbe olmasına bağlı olarak rezonans frekansında kaymalar ölçülüp, Sauerbrey denklemine göre adsorbe olan gaz miktarı belirlenmiştir. Iç içe geçmiş taraklı elektrotlardan gaza bağlı ve 1 mikroamper akım sınırlaması olarak sonuçlar alınmıştır.

İç içe geçmiş taraklı elektrot ve QCM tekniği kullanılarak altın katkılamanın polipirol tabanlı iletken polimerlerin gas algılama özelliklerine olan etkisi incelenmiştir. PPy, Fc, PPy-Fc, PPy-Au ve PPy-Fc-Au dan bir seri oluşturulmuştur.

Polipirolün Fc ile modifikasyonu, PPy-Fc'nin duyarlılığı PPy ye göre azalmış fakat Fc ye göre artırmıştır. PPy-Fc altın katkılamakla CO2 e duyarlılık PPy-Fc ye göre artmıştır. Karbondioksite karşı olan duyarlılık, PPy-Fc altın katkılamakla artmış fakat PP ye altın katkılamakla PPy ye olan duyarlılık azalmıştır.

Amonyak gazına karşı olan duyarlılık polipirolun ferosenle modifikasyonu ferosene göre artmış. Oksijene karşı olan duyarlılıkaltın katkılanmış PPy-Fc de PPy, Fc ve PPy-Fc ye göre daha fazladır fakat amonyağa karşı olan duyarlılık katkılama ile polipirole yakın bir sonuç çıkmıştır ama bunu yanın da oksijene olan duyarlılık altın katkılama ile ferosen ile modifikasyona göre artmıştır. Sonuçlara göre PPy, PPy-Au, Fc, PPy-Fc amonyağa karşı seçici davranmıştır.

1. INTRODUCTION

We live in an atmosphere containing so many kinds of chemical species. They can be artificial or natural. The effects of these chemical species can be harmful for our lives depending on their concentration Yamazoe [1]. At the present time, as a result of industrial applications and household waste, lots of dangerous substances such as toxic and combustible gases are produced. Inevitably, hazardous gases create a potential hazard for both plants and people living nearby. The widespread events such as asphyxiation, explosions and loss of life remind us importance of this problem. Therefore, gas sensors, helping us to overcome aforementioned problems, are indispensable for modern technological processes, in which analysis and control of gases are necessary [1-3]. Gas sensors are being widely used in the following areas: environmental, scientific and engineering research organizations; petrochemical and chemical industries; food and drink processing; medical institutions, including hospitals; microelectronics, including telecommunications and semiconductor manufacturing; power generators; and fabrication industries, including shipyards, engine and aircraft industries, etc.

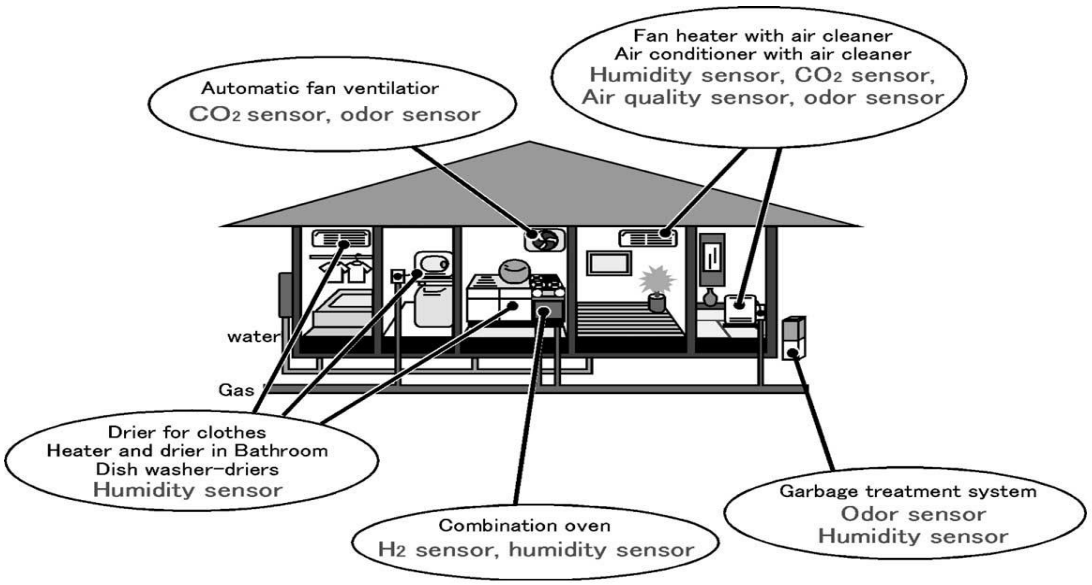

Figure 1.1 : Different types of gas sensors equipped in a house [4]

In this regard, nano materials have a pioneering role in gas sensor applications. Gas sensors utilizing these materials are designed to improve their features such as selectivity, response time, accuracy, precision, resolution, sensitivity, reproducibility and linearity. Here, nanocomposite films are attractive candidates with their novel properties. Especially, conducting polymers along with some additive materials are hot research subjects for gas sensing applications. To get higher conductivity in conducting polymer materials, metal atoms or metal oxides are added [5-7]. Some gases have higher affinity to certain metals. Gas molecules surrounding metal atoms, expected to change sensing properties of composite materials.

Among the conducting polymers, polypyrrole is a heterocyclic organic polymer, which is intrinsically insulating but can be made conductive by doping with a counter anion. In this respect, polypyrrole was doped with gold nanoparticles and also functionalized with ferrocene molecules in order to increase conductivity due to interaction of gases.

For this study, carbon monoxide (CO), carbon dioxide (CO_2), ammonia (NH_3) and oxygen (O_2) are used. Features, sources and effects of these gases except O_2 are shown in the Table 1.1.

Table 1.1 : Properties of toxic gases used in thesis

Gases	Features	Sources	Effects
CO_2	Colorless, odorless and nontoxic gas	combustion, cement production, respiration of animals, including people, the motor vehicle and industry, especially power generation	Greenhouse gas in the atmosphere. Create an oxygen deficiency and can result in asphyxiation or suffocation
CO	Colorless, odorless, flammable non-irritating, very poisonous	Produced by incomplete combustion of fuel such as natural gas, coal, or wood. Vehicular exhaust.	It restricts the blood's ability to carry oxygen. Little quantity bring about dizziness, headaches, fatigue, and slowed reaction times. It weakens the convulsion of the heart in a healthy person as well as decreases their capability to do exercise. Fetuses, newborns, and pregnant women are more susceptible to the effects. Large amounts are fatal.
NH_3	Pungent odor	NH_3 released from agricultural process. It is produced by the decomposition of animal manures.	Dangerous and caustic. Respiratory tract irritant. Above 1,500-ppm cause pulmonary edema, a possibly fatal hoarded of fluid in the lungs.

Quartz crystal microbalance (QCM) is an acoustic wave technique exploiting properties of the piezo electric effect. An AC voltage is applied across the piezoelectric quartz crystal. The crystal oscillates at its own resonant frequency, normally between 10 MHz and 30 MHz [8]. The three-dimensional waves produced travel across the entire bulk of the crystal. The thin film material deposited onto the surface of the crystal adsorbs gas molecules when exposed to various gases resulting in an increase in its total mass. This added mass varies the resonant frequency of the quartz crystal used for the sensing of gases.

Interdigitated electrodes (IDE) are used to detect variations in resistivity of coated thin films involving electronic charge transport within the conjugated electronic states of the conductive polypyrrole when exposed to different gases at room temperature.

In the scope of this thesis, effects of gold nanoparticle doping on the sensing properties of polypyrrole based conducting polymers were investigated against CO, CO_2, O_2 and NH_3 by means of acoustic wave and electrical based techniques. Gas measurements were conducted in an electromagnetically shielded and hermetically sealed measurement cell specifically designed to acquire QCM and electrical signals from the electrodes. The thin-film coated electrodes were exposed to varying concentration levels of CO, CO_2, O_2 and NH_3 ranging from 0 vol% to 100 vol% in 5 intervals by using a computer controlled mass flow meter array. The frequency shifts of the vibrating quartz crystal from its natural resonant frequency due to gas sorption of the thin-film coated QCM electrodes was measured. These shifts were then converted to sorbed mass according to the Sauerbrey relation. The resistance changes through thin-film coatings on the interdigitated electrodes were measured under a compliance current value of 1.0000 mA.

1.1. Gas Sensors

Sensors are devices that convert the physical and chemical changes in to electrical signal. Sensing technology is widely used in gas detection fields. Recently, gas sensing, used within intelligent systems, is attracting great attention in both academia and industry because of their wide use in different fields. Firstly, gas sensors are industrial products [9-27]. For instance, they are used for detection of methane in

mines. They are also used in automotive industry as detectors for polluting gases or unburned fuel [28-42]. Medical applications are one other application field as electronic noses, which simulate the human olfactory system. Gas sensors are also used for the supervision of indoor air quality [43-54]. Gas sensors are frequently used to monitor greenhouse gases [54-56]

1.1.1. Characteristic of ideal gas sensors

There are several aspects for a gas sensor that should be taken into account in order to attain optimum sensor quality. These are sensitivity, selectivity, stability, detection limit, dynamic range, linearity, resolution, response time, recovery time life cycle, hysteresis and life cycle.

- ✓ Sensitivity is defined as the ratio between the change of measured signal and analyte concentration unit. In other words, it is the gradient of the graph of calibration.
- ✓ Selectivity means whether a gas sensor is able to respond the analytes in some definite specification.
- ✓ Stability is defined as the capability of a sensor to reproduce same outcome for a specific period of time, responding to any gas.
- ✓ Detection limit is defined as the minimum rate of gas concentration that can be detected by the gas sensor for some condition especially at specific temperature.
- ✓ Dynamic range is the range of the gas concentration between the lowest and highest rate of analyte concentration
- ✓ Linearity, how the calibration graph according to the experiment is shaped like (the more the graph seems to be linear, the more quality a gas sensor is)
- ✓ Resolution is how low a gas sensor is able to distinguish the analyte concentration.
- ✓ Response time that is needed for a sensor to rise the concentration from zero to a certain value of concentration.
- ✓ Recovery time is the time required to return the sensor signal to its initial value after a step concentration change from specific value to zero.
- ✓ Working temperature is the temperature when the maximum sensitivity occurs.

Based on these aspects, in order to a chemical sensor be ideal, it should bear perfectly sensor qualities. Most of the investigators usually do not try to attempt to cover all of the proportional aspects. They only pick some of these ideal aspects and ignore the others. This is because the objective of creating a sensor that is ideal for some gases is extraordinarily difficult, if not impossible. On the other hand, real life applications typically do not need sensors with perfect specifications at once. For example, a sensor device that is used to detect the concentration of a spacimen in an industrial process does entail a detection limit at the ppb level, although the response time within seconds or less would be suitable. In an other case, in environmental monitoring applications, the requirements of the detection limit can be much higher when the concentrations of contaminants normally and gradually change, nonetheless response time of a few minutes can be suitable. Therefore, the investigators seem only to pay attention on how useful those aspects are for each application.

1.1.2. Types of gas sensors

1.1.2.1. Semiconductor gas sensors

Semiconductor gas sensors, usually known as metal oxide semiconductor gas sensors, contribute gas sensor field with low cost and high sensitivity. Metal oxide semiconductor gas sensors are basically used to distinguish target gases through redox reactions between target gas and oxide surface[55] at high temperatures above 200^0 C. This process classified into two step [56]: (1) redox reaction react with target gas and surface which O- was distributed on. As a result of that, variation occurs on oxide surface. (2) Then, this variation is converted into an electrical signal so as to be monitored as sensor output. The resistance variation can be detected as change of capacitance, mass, work function, reaction energy or optical characteristic [57]. Beside all these, redox reaction mentioned above usually takes place temperature between 200 and 250 ^{0}C.

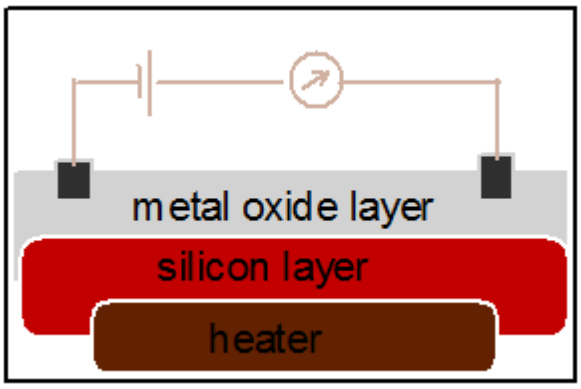

Figure 1.2 : Basic components of metal oxide based semiconductor gas sensor

1.1.2.2. Field effect transistor (FET) gas sensors

In semiconductor materials, electric field is used as control tool to change conductivity of materials. But, it can control only one type of charge carriers in semiconductor. That is the basic working principle of field effect transistors (FET). The FET devices convert variable chemical and physical quantity into electrical current. For different purposes, many FET devices were developed. For gas sensor application, metal oxide semiconductor field effect transistors (MOSFET) are widely used. Basic structure of FET device consists of source drain and gate on the silicon oxide insulator. Gathered signal comes from material between source and drain. The signal monitored as I-V characteristic of material. Variation signal depends on gas concentration of the environment.

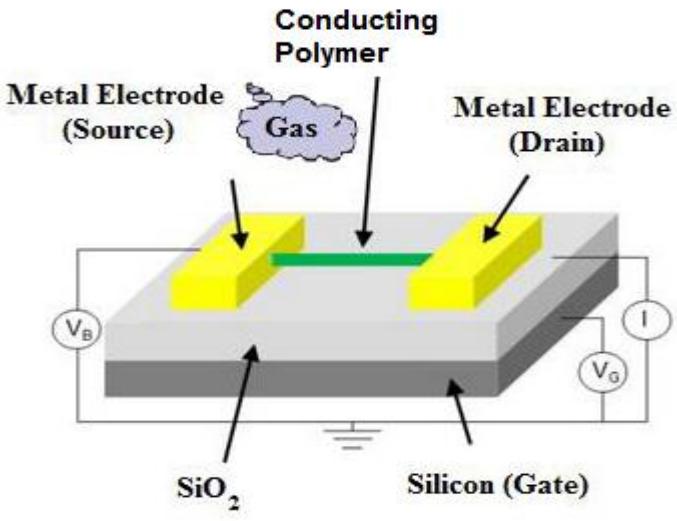

Figure 1.3 : Basic structure of FETs [58]

1.1.2.3. Optical gas sensors

Sensors based on optical methods are usually simplistic. Their results are quite reliable because of higher stability, sensitivity and selectivity than non-optical sensors with longer lifetime. Optical gas sensors are frequently used for chemical and biological applications. Response time is relatively short, which enables real time detection. Environmental changing, catalyst poisoning effect by certain gas do not effect of the optical gas sensors' performance. Their sensing methods for sensor applications mainly based on spectroscopy. On the other hand, miniaturization problems and higher cost really restrict their application on gas sensors. Consequently, merely a few marketable gas sensors are based on optical principles. In the Figure 1.4, an optical system, used for NO_2 sensing application, was displayed [59].

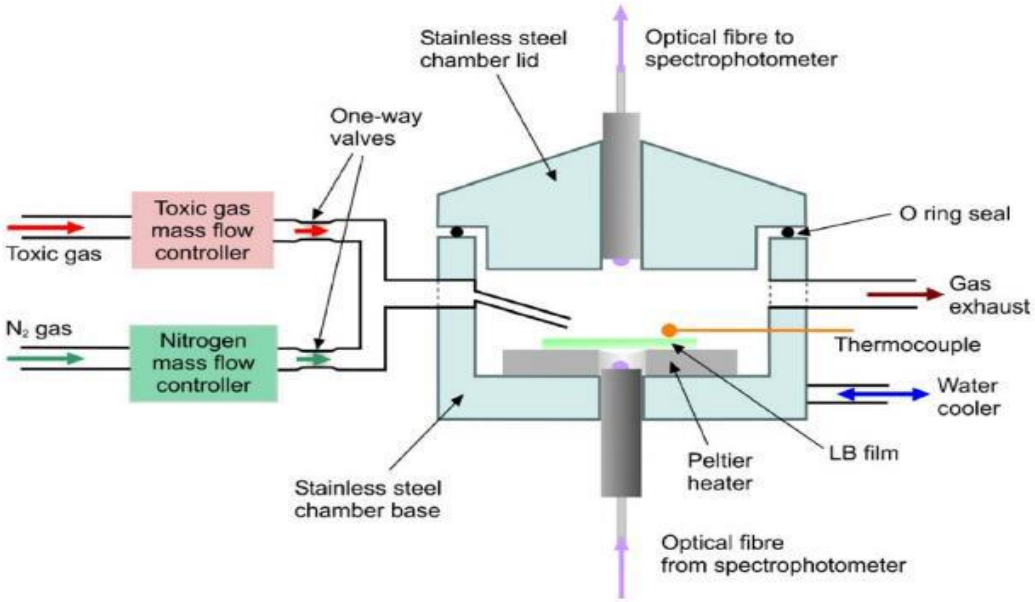

Figure 1.4 : Optical gas sensor system

1.1.2.4. Electrochemical gas sensors

Electrochemical gas sensors are mainly used for detection of oxygen and toxic gases. Electrochemical sensors are basically fuel cells made of gold or platinum electrode in an electrolyte. The electrolyte is an aqueous solution of strong acids. When the cell detects a gas a small current is generated which is proportional to the concentration

of the gas. In its simplest form, electrochemical gas sensors are composed of a diffusion barrier, a counter-electrode (cathode), a sensing electrode (working-electrode, anode) and an electrolyte. In an environment with no chemically reactive gases, oxygen diffuses into the cell and adsorbs on both electrode. Whereas theoretically no current is expected, a process is resulted with a little current flow. Actually, there is a stable potential voltage between both electrodes.

Relaying on the gas type, oxidation or reduction of the gas occur while gas move through barrier and therefore current flow happens due to potential difference between two electrodes.

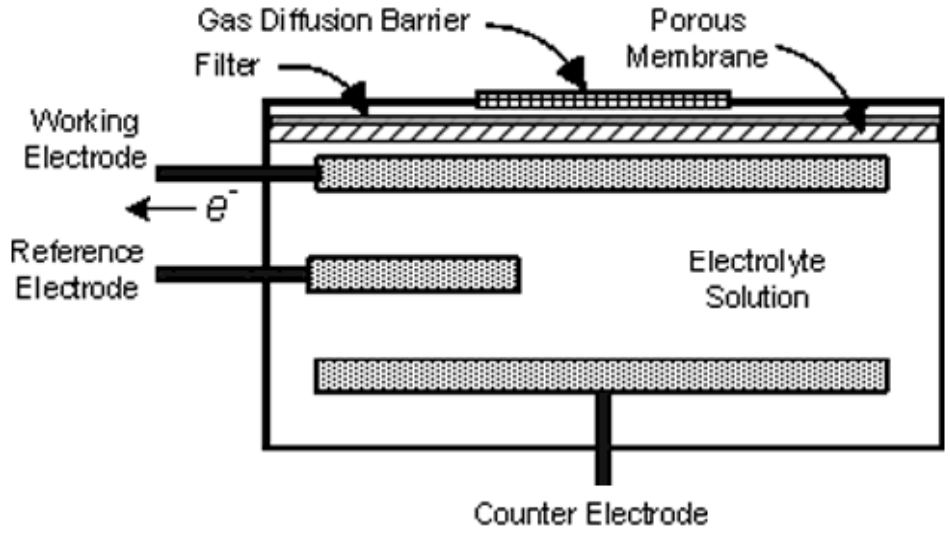

Figure 1.5 : Schematic wiev of electrochemical gas sensor [60]

1.1.2.5. Catalytic gas sensors

In recent years, catalytic gas sensors are mostly demanded and widespread gas sensor. This type of sensors composed of a platinum warmer wire occupied on a gas permeable ceramic carriage. Catalyzer (platinum or palladium) is spread to pave the way for burning of methane gas on the ceramic carriage. Sensor temperature is kept the level of the catalyzer surface to oxidize the methane encountered with by applying voltage continuously. During the combustion of methane with the help of catalyzer on surface, emerging energy increase sensor's temperature, therefore it increases the resistance of platinum heater. Amount of the released energy and increase resistance of heater is directly proportional to the amount of methane or other hydrocarbon-based explosive combustible gases in the air. According to the

working principle, catalytic gas sensors are selective just for hydrocarbon-based gases such as methane, ethane, etc.

1.1.2.6. Piezoelectric gas sensors

Piezoelectric sensors are differentiating as surface acoustic wave (SAW) sensors and quartz crystal microbalance (QCM). QCM produces a wave that goes through the bulk of sensor while the SAW sensors produce surface wave that move surface of sensors. Both of the sensor types have same working principle. A variation in the mass of piezoelectric sensor coated by sensing material due to gas adsorption leads to variation in resonant frequency [61].

1.2. Conducting Polymers

1.2.1. History of conducting polymers

Polymers have a big role on today's modern life. Even though being in our lives since the 1920s, there was not much scientific study on polymers. Chemists have started to study on that subject after Staudinger came up with polymer term firstly.

In the 1970s, with the accidental discovery of doped polyacetylene, the first conducting polymer [62], a new kind of research area called conducting polymers was born..

1.2.2. Application of conducting polymers

Conducting polymers can be used in different fields due to their electrochemical properties. They are widely utilized in rechargeable batteries, photoelectrochemical cells, electrochromic devices, and ion-selective electrodes. Conducting polymers are also used in sensor applications. These polymers can be obtained at low cost, and only the initial units are designed and a number of features can be regulated such as electronic properties, optical properties, conductivity properties and hardness. They were used in diverse fields such as light emitting diodes [63-65], photovoltaic devices [66-70], transistors [71-74], and molecular electronic devices [75-77].

Being applicable promisingly in so many fields, conducting polymers attracted attention of scientist for last 30 years. Furthermore, compared to other inorganic

electrochromic materials, polymers have many outstanding features. Some examples of these features can be counted as follows. They can be coated onto large surfaces by spinning, spraying or printing methods. They might get more than one color from only one material. In addition to having high redox stability, they have lower response times. Due to all of these outstanding features, conducting polymers are used widely on electronic devices [78, 79], optical screen [80], electrochromic glasses [81, 82], electrochromic mirrors [83] and camouflage materials[84]. For these reasons, for design and synthesis of organic π-conjugated polymeric electrochromes many investigations have been carried out.

1.2.3. Electrical properties of conducting polymers

The simplest version of conjugated polymers is polyacetylene consisting of a basic carbon skeleton. The basic structural feature of all conjugated polymers is their quasi-infinite π-system and delocalized π-system extending over a wide range of recurring monomer units. These properties provide electrical conductivity to polymers with long polymer chains. Delocalization of polyacetylene is twice degenerated than the basic structure.

Energy differences between single and double bonds in aromatic polymers such as poly (paraphenylene) result in alteration in electronic structures of polymers.

In a polymer, as in case of an entire crystal, interaction between unit cells into the polymers and units next to the polymers lead to formation of electronic bands. These bands are known as highest occupied molecular orbital (HOMO) or valance band (VB) and lowest unoccupied molecular orbital (LUMO) or conduction band (CB). If band gap formation occurs under 3 eV or 4 eV, these polymers are called semi-conductor (Polymers are insulator under higher eV values). By definition, band gap is known as the differences between VB and CB. Another definition states that band gap is equal to smallest excitation energy which corresponding to small energy value in the last part of absorption spectrums. A polymer to be a semi-conductor with large band gaps, it is essential to increase electrical conductivity by constituting charge carriers in the polymers. An example would be poly (paraphenylene) which has electrical conductivity of 500 Ω^{-1} cm^{-1} when doped with charge carrier and 10^{-13} Ω^{-1} cm^{-1} when non-doped. Charge carriers are either positive or negative and they are the

product of oxidation or reduction reaction of polymers respectively. This phenomenon always accompanies some localized structural changes on ring pairs and result in creation of new electronic levels. The beginning of the formation of charge and geometrical distortion cause electronic movement which known as polaron for aromatic polymers. Formation of charge and radical form depends on sorts in the bond. Any increase in the distance between bonds entails the formation of quinoids at higher energies. Removal of second electron from molecule brings about formation of new polaron or it is possible to create bipolaron by removing of second electron from same group. As the level of doping increase, energy level of polaron and bipolaron tend to merge.

1.3. Theoretical Foundations

1.3.1. Piezo-electric effect and quartz crystal microbalance theory

Piezoelectric effect was totally described by Pierre and Jacques Curie for the first time in 1880. Currie brothers observed that tourmaline, quartz and potassium sodium tartrate have crystal structures that produce electrical responses because of stress and strain applied at specific directions. In contrast to this effect, materials like quartz deforms mechanically by applied electrical signals [85]. Resulting mechanical distortion is proportional to the applied electric field intensity. Although the resulting piezoelectric voltage and the magnitude of the force are very small, we can see piezoelectric materials in a wide range of usage such as submarine sonar sensor applications. Piezoelectric materials can be divided in to two main groups such as ceramic and crystal materials. While crystal structures show natural piezoelectric effect, ceramic materials known as piezoceramics have an artificial piezoelectric effect. The most known piezoceramic materials are barium titanate ($BaTiO_3$) and lead zirconate titanate (PZT). Barium titanate's Curie temperature is 120°C. PZT's Curie temperature can range between 150°C and 200°C.

For the first time Sauerbrey claimed that piezoelectric effect can be used as a mass sensor. Changes in the mass of material deposited on the crystal surface cause shift of crystal's resonance frequency. Sauerbrey discovered that frequency shifts of a crystal is independent from the deposited material's physical properties [86]. Mass changes on crystal can be observed, without the necessity of knowing the physical

properties of deposited materials, from the simple measurement of the frequency shift. Quartz crystal microbalance technique, based on basic physics, constantly is used some field like thin film coating, thickness monitor and so many sensor application. QCM technique is based on the measurements of the frequency shift of the qcm electrode coated by gold thin film. QCMs were used to determine the thickness of thin films at 1960s and 1970s. At very simple principle, they can be used as gas sensor as a result of the sensing of gas molecules by sensitive receptor occupied on electrode [87, 88]. In this method, quartz crystal, one of the most abundant minerals in nature, is used as an oscillator. Pure silisium dioxide (SiO_2) crystal is called as quartz. Its melting point is 1650 °C and specific weight is 2.65 g/cm^3. When the silisium dioxide is heated up to 573 °C, called transition temperature, crystal structure changes. Quartz is named as beta-quartz if crystal structure formed above the transition temperature and called alpha-quartz formed in rest temperature. For resonator application, only alpha quartz is preferred because it is superior in terms of mechanical and piezoelectric properties.

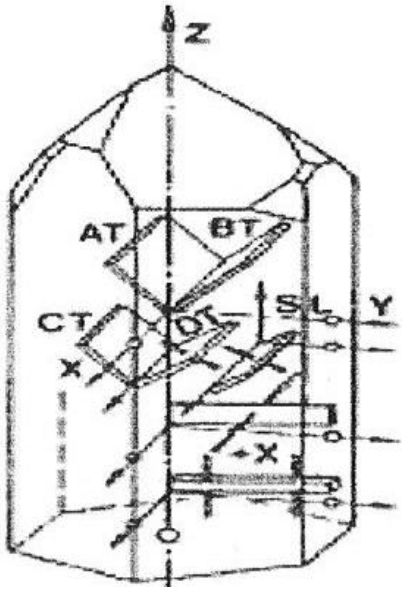

Figure 1.6 : Different quartz crystal cut angels

Vibration frequency of quartz crystal to be used as resonator depends on the cutting angle during the production. Cutting angle determines the mode of the quartz's vibrations according to the selected application requirements. Typically, AT cutting, BT cutting, SC cutting, IT cutting and FT cut crystals are used for different application purposes. AT cut crystals are mostly used for qcm electrodes and

oscillates in the thickness shear mode. AT cutting quartz crystal is cut magnitude of angle 350° 5′, 350° 10′or 350° 15′ with respect to pure quartz crystal's z axis.

The frequency of preferred crystal oscillators for gas sensor applications are mainly between 5 MHz and 30 MHz. High frequency quartz crystals need thinner crystal but they have fragile structure. Resonance frequency variations with temperaturefor different cut angles of pure quartz are given. For so many applications AT cut quartz is cut at an angle of 35°15′ with respect to y-z axis. Electronic equipments produce heat between 500 °C and 600 °C. For that temperature AT cut quartz is more suitable because it has the smallest temperature coefficient. AT cut quartzs with 35° 10' angle are more commonly used for detection. For this kind of quartz's temperature coefficient is nearly zero between the temperature 0 and 500.

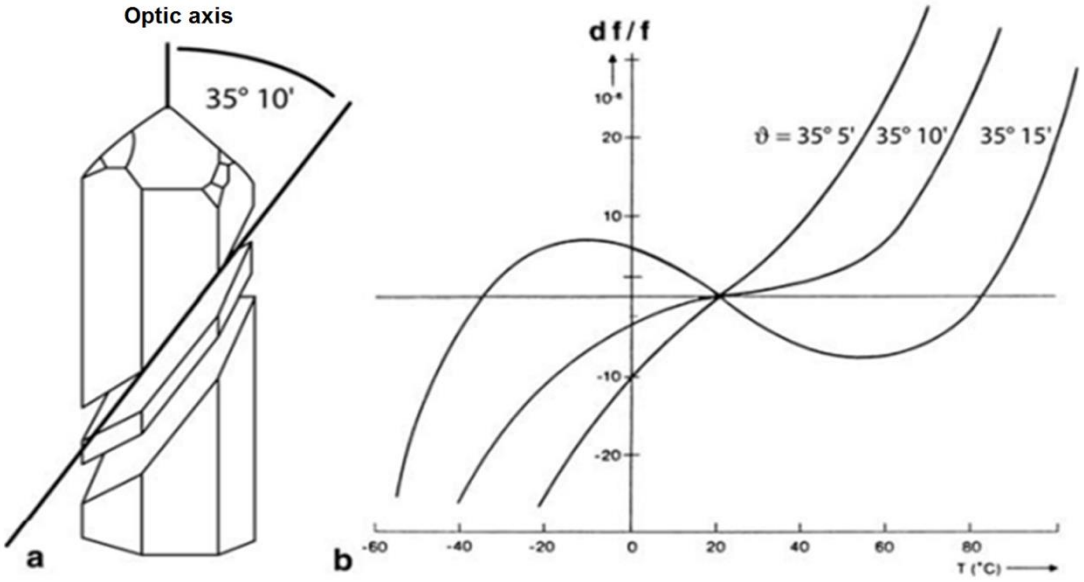

Figure 1.7 : Quartz crystal's (a) AT-cutting angle and (b) natural vibration frequency, temperature and cutting angle relation.[89, 90]

AT cut quartz is the best choice for QCM applications because of its properties [91]. In the QCM technique, mostly disc shaped and 5 MHz and 30 MHz oscillators are used. Vibrational frequency (f_R) is also determined by the thickness of the crystal. Gold electrodes, on both sides of the QCM electrode and produced by lithographic methods or vacuum deposition methods, does not interact with oxygen and receptor materials. QCMelectrodes are used to stimulate the acoustic waves. Receptor chemical material which will interact with the gas analyte is coated as thin film on this electrodes by using any coated methods.

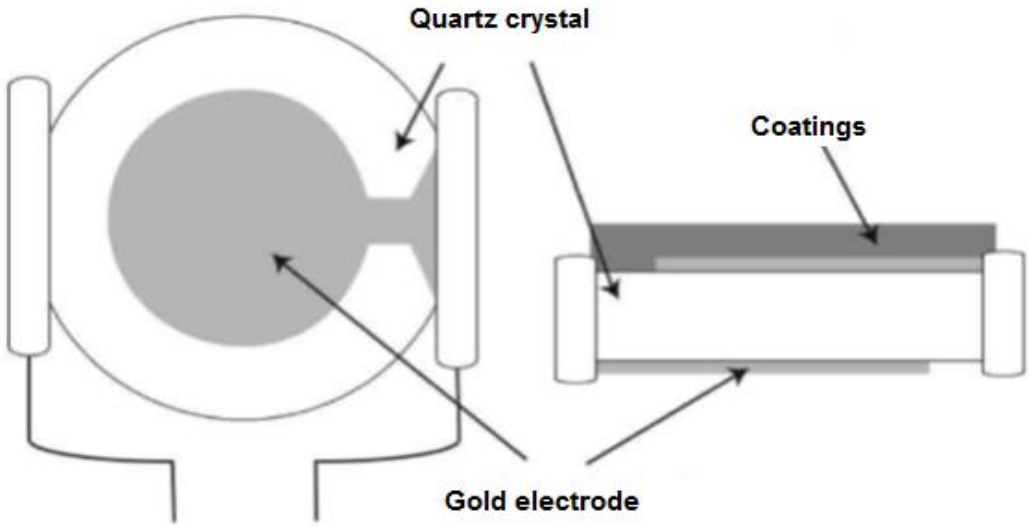

Figure 1.8 : Quartz Crystal Microbalance gold electrode

M stands for mass and t stands for thickness. At the resonance condition, wavelength λ:

$$\lambda = \frac{2t}{n} \quad \textbf{(1.1)}$$

For n=1 frequency (f) and for higher harmonics n value is bigger than one, so shear velocity v is defined as:

$$v = \lambda f \quad \textbf{(1.2)}$$

So frequency is equal

$$f = \frac{v}{2t} \quad \textbf{(1.3)}$$

Due to a very small change in thickness of the resonance frequency shift can be found by differentiation of both sides of the above equation.

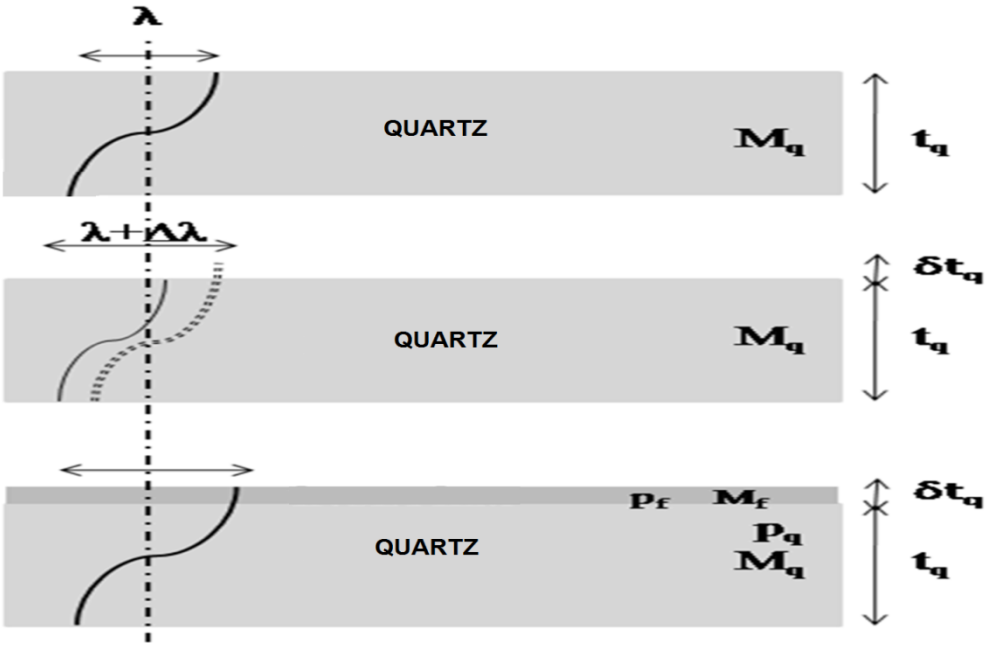

Figure 1.9 : The wave advancement of thin-film-coated quartz crystal electrode

So

$$dF = -\frac{v}{2t^2}dt \qquad \textbf{(1.4)}$$

We will find relative change if we divide above equation by than above one:

$$dF = -\frac{dt}{t} \qquad \textbf{(1.5)}$$

Thus in the above figure, relative change in thickness of the crystalline resonance frequency was reduced. Mass M per unit area coated material and the amount of change in mass per unit area in ΔM written as:

$$\frac{\Delta F}{F} = -\frac{\Delta M}{M} \qquad \textbf{(1.6)}$$

The net change in mass ΔM was assumed co-distributed over the surface area in this derivation. Hence, change in mass per unit area is proportional to the change of all mass ΔMcrystal over the crystal surface. This means that shear rate is the same over the entire crystal surface. M and ΔM are written in terms of the density of materials per area on the thin film (ρf) and in terms of thickness (tf).Relative change in resonance frequency:

$$\frac{\Delta F}{F} = \frac{-\rho f\, tf}{\rho t} \qquad \textbf{(1.7)}$$

The resonance frequency F=v/2t is put proper place then the above equation:

$$\frac{\Delta F}{F} = \frac{-2F\rho f\, tf}{v\rho} \quad \textbf{(1.8)}$$

Or

$$t_f = -\frac{\Delta F}{2F^2}\frac{v\rho}{\rho f} \quad \textbf{(1.9)}$$

found.

F, ρ, and v values are constants as result of production of electrode. Above equation says that if the density of coated material is known, QCM will be used as a thickness monitors.

We can find crystal constant

$$C_q = \frac{2}{v\rho} \quad \textbf{(1.10)}$$

So the relationship between the frequency offset and mass

$$\Delta F = -C_q\, F^2\, \Delta M \quad \textbf{(1.11)}$$

can be written.

Therefore, changes in the resonant frequency:

$$\frac{\Delta F_p}{F} = C_q F \Delta M_f \quad \textbf{(1.12)}$$

Equations reduced this form finally. Below equation is known as Sauerbrey [86]. Different derivation of this equation and impressions are also available. Change on the stored material on crystal can be determined only by measured resonance frequency shift without dependence on the material's physical properties. So, change in frequency is directly related with change in mass.

$$\Delta f = \frac{-2f_0^2}{A\sqrt{\mu\rho}}\Delta m \quad \textbf{(1.13)}$$

Here, QCM crystal's natural vibration frequency is f_0. A is area of coated gold on qcm crystal. μ is shear stress of quartz and ρ represents density of crystal.

Sauerbrey equation was developed to check only vibration properties of coated solid material on electrode in air condition.

QCM has been used only gas phases application until 1980. QCM measurements were performed in the liquid phase in 1985 and it was shown that qcm electrode can be

vibrated steady in completely fluid-filled environment. It is indicated that resonance frequency shift is proportional to the liquid density multiply viscosity.

1.3.2. Non-linear (Positive) QCM response

Interaction between analite and adsorbed materials generally cause frequency decrease or negative frequency shifts on QCM electrode as stated Sauerbrey [89]. However, in some conditions, some sensing materials shows positive frequency shifts even though they adsorp gases. It may be discribed according to visco-elastic changes in mechanical stiffness of sensing materials.

Sauerbrey equation explains relation between frequency shifts of quartz crystal and mass of sorbed materials on QCM surface. Nevertheless, the Sauebrey equation is merely appropriate for the case when adsorbed materials mass is much lower then the initial frequency of electrode and mass deposited to the quartz crystal surface oscillating with quartz at the same frequency. Coated oscillating film ought to have same wave velocity with the quartz crytal surface. Sauerbrey equation shows lineer relationship between frequency shifts and mass uptake without considering deposited films' physical properties. QCM frequency decreases while uptaking mass on films. But, in some cases, non-linear behavior of QCM results are seen [92-94]. In fact, perturbations in the physical and mechanical characteristics of the deposited film or material on the quartz crystal bring about nonlinear or positive response in the resonance frequency of a quartz crystal. Hunt et al.[95-97] bring into existence an equation from time-dependent perturbation theory to explain positive QCM frequency as;

$$t\frac{\partial \Delta\omega}{\partial t} + \Delta\omega = \frac{\omega_u h_f}{\pi\sqrt{\rho_q \mu_q}} \times \left[-\omega_u\left(\Delta\rho - \frac{\Delta\mu}{V_s^2}\right) + j\left(\frac{\partial \Delta\rho}{\partial t} - \frac{1}{V_s^2}\frac{\partial \Delta\mu}{\partial t}\right)\right] \qquad (1.14)$$

where h_f is the film thickness, ρ_q is mass density of quartz crystall, V_s is acoustic wave velocity across the deposited film section, ρ is density of film, and μq is shear stiffness of quartz, μ is the stiffness of the thin film, Δ is difference between perturbed and unperturbed quantities, and subscript u is used to indentify unperturbed quantities. Assuming Δρ, Δμ, and Δω are constant with time and omitting kinetic changes, Equation 1.15 can be rearranged as following;

$$\Delta f = -\frac{2f_u^2 h_f}{\sqrt{\rho_q \mu_q}}\left(\Delta\rho - \frac{\Delta\mu}{V_s^2}\right) \quad (1.15)$$

Since μ and ρ are constant, the mass uptake can be defined as $\Delta m = \Delta\rho A h_f$ (A being the sensing area), the first term of Equation 1.15 is the Sauerbrey equation covering static changes in the mechanical stiffness of the deposited film. This relation correlates negative frequency shifts with attached mass on the QCM sensor (first term), whereas positive frequency response to the mechanical stiffness of the film (second term). Another effect that cause a deviation from the Sauerbrey equation may result from liquid clusters forming by condensation on the coated quartz crystal. In this case, an initial drop in the frequency shift is accompanied by a subsequent increase due to liquefaction of the adsorbate.

1.3.3. Adsorption kinetics

In the adsorption process, an adsorbed molecule is bound in a low energy state. This low energy level is a combination of an active surface site hosting the adsorbed molecule. Adsorption phenomena was explained in reference [98] in literature in details.

The solid's surface is composed of identical active sites that will be accommodated by active species, which is denoted by 's'.

Then adsorption can be considered as an actual chemical reaction, where the following notations will be used:

- [A] represents a compound A in gaseous state,
- << A >> is for a constituent A in a solid or gas environment,
- < A > is for a pure solid or gas phase of compound A.

In this case, the adsorption reaction is written as:

$$[G] + << s >> \Leftrightarrow << G - s >>$$

Here, << G – s >> is the new species formed, and therefore a G – s will exist in gas concentration 's'.

1.3.4. Thermodynamic model of the langmuir adsorption isotherm

If the mass flow law is applied to the previous adsorption equilibrium reaction,

$$K = \frac{|<<G-s>>|}{P|<<s>>|} \tag{1.16}$$

where K is the equilibrium constant. It is expressed by,

$$K = K_0 \exp\left(-\frac{\Delta H^\circ}{RT}\right) \tag{1.17}$$

Adsorption is an exothermic process, accompanied with a negative enthalpy change ($\Delta H^\circ < 0$). A negative value for ΔH° means that if the temperature increases the reverse reaction occurs. Thus, adsorption is favored at low temperatures.

In an ideal solution, if S represents the number of free sites, S_0 means the number of sites, and θ indicates the fraction of sites that are in use, which is expressed as,

$$\theta = \frac{S_0 - S}{S_0} = |<<G-s>>| \tag{1.18}$$

then,

$$|<<s>>| = \frac{S}{S_0} = 1-\theta \tag{1.19}$$

which yields,

$$K = \frac{\theta}{(1-\theta)P} \tag{1.20}$$

and therefore,

$$\theta = \frac{KP}{1+KP} \tag{1.21}$$

This relation, called the Langmuir isotherm, expresses the percentage coverage of the surface as a homographic function of pressure. This function is a proper relation to represent most adsorption-related experimental results.

An important aspect of this relation is that, at low surface coverage fractions ($\theta << 1$), a proportionality law similar to Henry's law is obtained, where $\theta = KP$.

1.4. Materials

1-(2-cyanoethyl) pyrrole and ferrocene aldehyde were obtained from Aldrich Chemical Co. All other chemicals were analytical grade and used without further purification. Electrochemical polymerizations and measurements were performed through a CHI Model 842B electrochemical analyzer. A small glassy carbon working electrode having 2 mm diameter, a platinum wire counter electrode (0.2 mm diameter), an Ag/AgCl-saturated KCl reference electrode, and a conventional three-electrode electrochemical cell were purchased from CH Instruments. Materials used in this thesis was synthesized by Dr. Mehmet Şenel at Fatih University. Ferrocene was purchased commercially.

1.4.1. Polypyrole

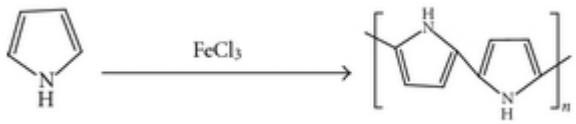

Figure 1.10 : Polypyrrole synthesis scheme

Polypyrrole was chemically obtained by mixing 2.881-gram pyrole monomer in 50 ml of 0.1 M FeCl3 solution. Synthesis reaction temperature was maintained at 5-7 ° C at approximately one hour. Then reaction has been gone on at room temperature for four hour. Precipitate obtained by synthesis was washed and was made dry at vacuum oven.

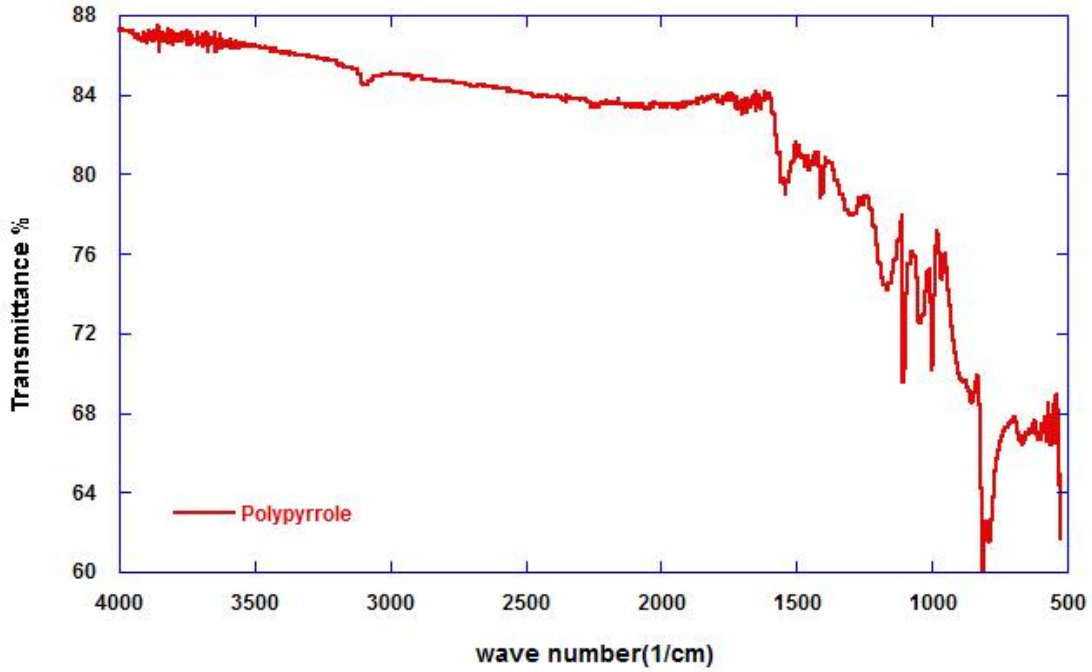

Figure 1.11 : FTIR spectra of polypyrrole

Approximately, between 3500 cm^{-1} and 3700 cm^{-1}, amine N-H stretch bonds can be observed as two peaks from FTIR spectra of PPy. Aromatic -C-H groups vibriations can be observed between 2900 cm^{-1} and 3100 cm^{-1}. Aromatic carbon-carbon double bond bending can be observed between 1500 cm^{-1} and 1700 cm^{-1}.

1.4.2. Ferrocene

Ferrocene, an organometallic compound is composed of two-cyclopentadienly and iron atom located between cyclopentadienly. Molecular structure of Ferrocene looks like sandwich shape. Ferrocene was purchased from Sigma-Aldrich.

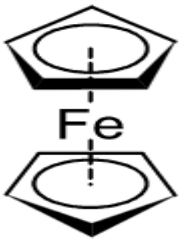

Figure 1.12 : Molecular structure of the Ferrocene molecule

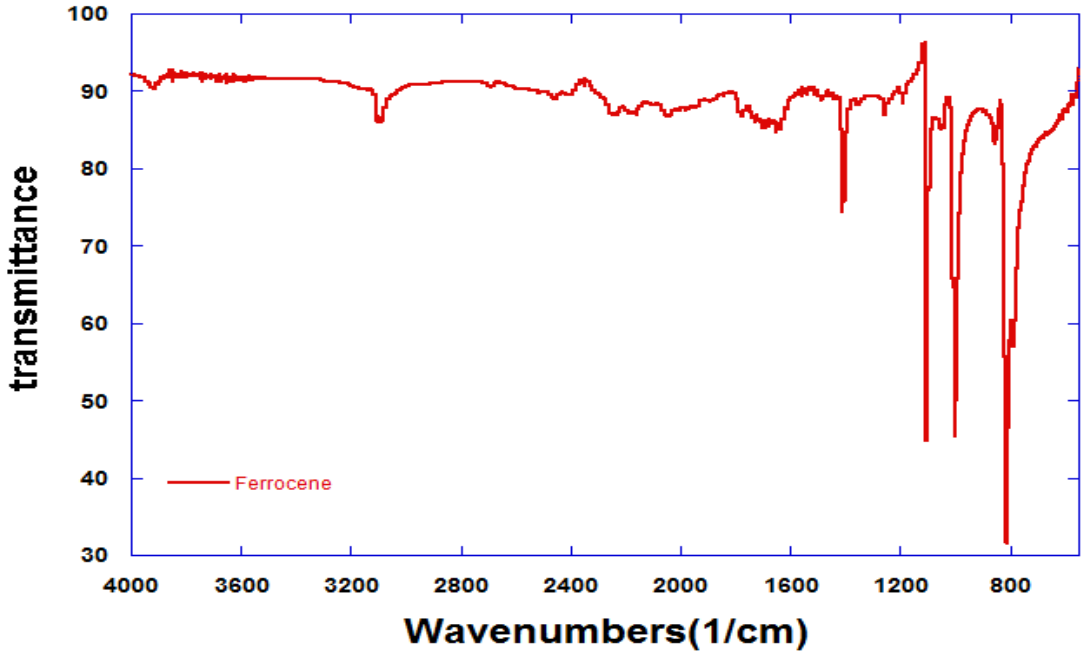

Figure 1.13 : FTIR spectra of Ferrocene

From the FTIR spectrum of Fc, peaks of alkenly (C-H) stretch can be observed between the value of 3000 cm^{-1} and 3100 cm^{-1}. Aromatic carbon double bonds bendings can be observed between the value of 1700 cm^{-1} and 1500 cm^{-1}. Aromatic C-H bonds bendings can be seen between the values of 700 cm^{-1} and 850 cm^{-1}.

1.4.3. Polypyrole-ferrocene

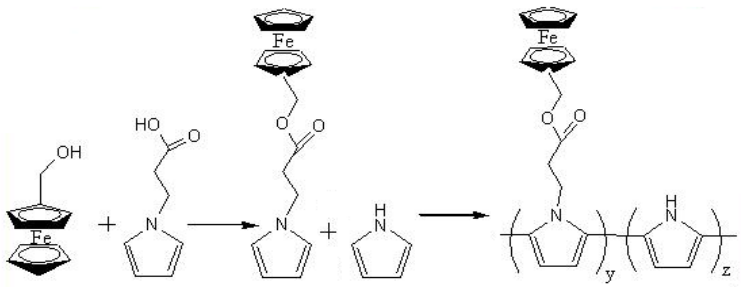

Figure 1.14 : Polypyrrole-Ferrocene's synthetic scheme

1-(2-carboxyethyl) pyrole was obtained by hydrolysis of 1-(2-cyanoethyl) pyrole (PPy-CN). 100 ml potassium hydroxide solution mixture, containing 25 gr PPy-CN, was stirred for 40 hours at 500 °C. Then the mixture was cooled at room temperature and HCI was added. After extraction with ether, raw product was obtained by evaporating of ether. Raw material was dissolved in ether and distilled by

crystallization. Solution of EDC (600 mg, 3.14mmol) in dichloromethane (4ml) was added drop by drop to ferrocene alcohol (750mg, 3.5mmol), 1-(2-carboxyethel)pyrole (500mg, 3,6mmol) and DMAP (30mg, 0.3mmol) solution in dichloromethane at 100^0C. After the addition, the reaction mixture was stirred under argon gas at room temperature for 20 hours. The reaction mixture was washed 3 times with 1 M NaOH and twice with purified water. The organic compound was separated by dehydrated magnesium sulfate and the solvent by vacuum. Yellow solid was obtained in ethanol by crystallization. The polypyrole-ferrocene monomer was obtained chemically by mixing pyrole-ferrocene and pyrole monomers in 50 ml, 0.1 M $FeCI_3$ solution. The synthesis reaction temperature was hold between 5 and 7^0C. Reaction was carried out in room temperature for 4 hour. The obtained precipitation was filtered and washed with pure water and was dried in vacuum oven.

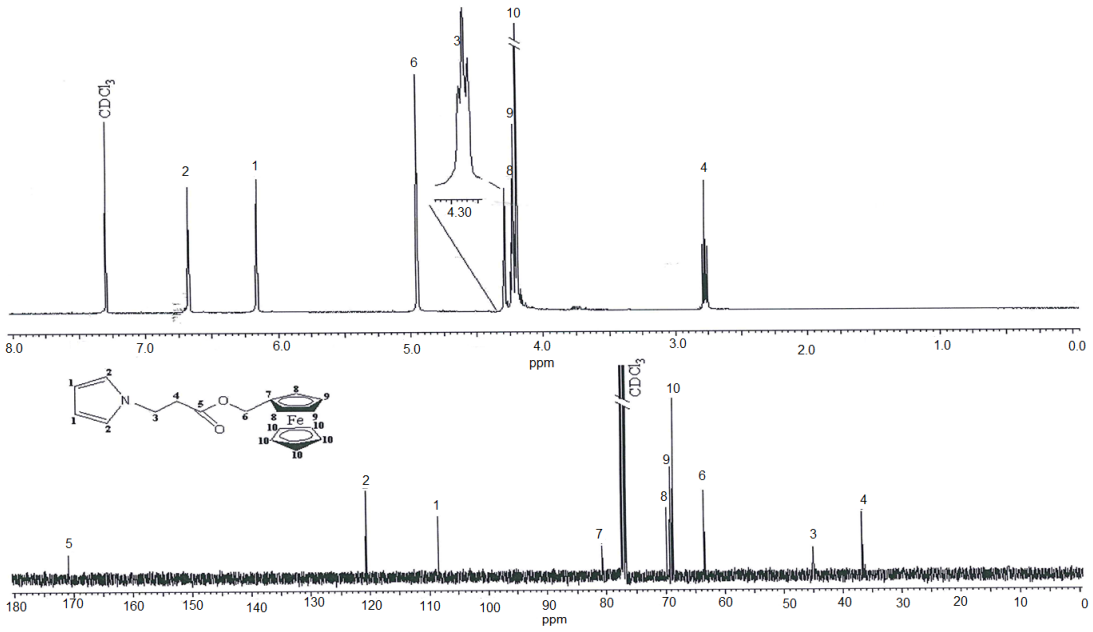

Figure 1.15 : NMR result of Py-Fc monomer [99]

Monomeric structure of Py-Fc was examined in ^{1}H and ^{13}C NMR. As indicated in Figure 1.15, the peaks of all structural properties of monomeric Py-Fc were determined. The most important signal in the Py-Fc spectrum is the signal of fracture of cyclopentadiene observed between 4.18-4.25 ppm. α and β protons of pyrrole were observed as two triplet at 6.16 and 6.66 respectively. Resonances derived from ethyl chains bonded to pyrrole were seen at 2.77 and 4.28 ppm respectively. Py-Fe ^{13}C NMR is illustrated in Figure 1.15. Signal at 171 ppm is due to the presence of

ester carbonyl carbons. Ethylene carbon atoms in pyrrole and carbon atoms in ferrocene were signaled at 37 (C3), 45 (C4), and 64 (C6) ppm. Carbon atoms in pyrrole indicated signals at 108 (C1), 121 (C2) ppm. Resonances belongs to Cyclopentadiene were appeared at 81 (C7), 69.7 (C8), 69 (C9), ve 68.6 (C10).

1.4.4. Polypyrole-Au nanocomposite

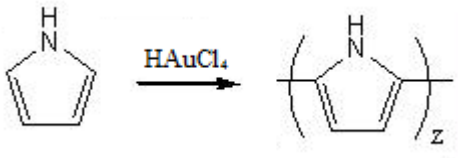

Figure 1.16 : Polypyrrole-gold nanocomposite synthesis scheme

Polypyrole Au nanocomposite synthesis was carried out by stirring at 2.5 µl 0.0125M $HAuCl_4$ solution and 2.5 µl 0.0925 M Py monomer solution for thirty minute. Then, it was filtered. The nanocomposite was dried in vacuum oven.

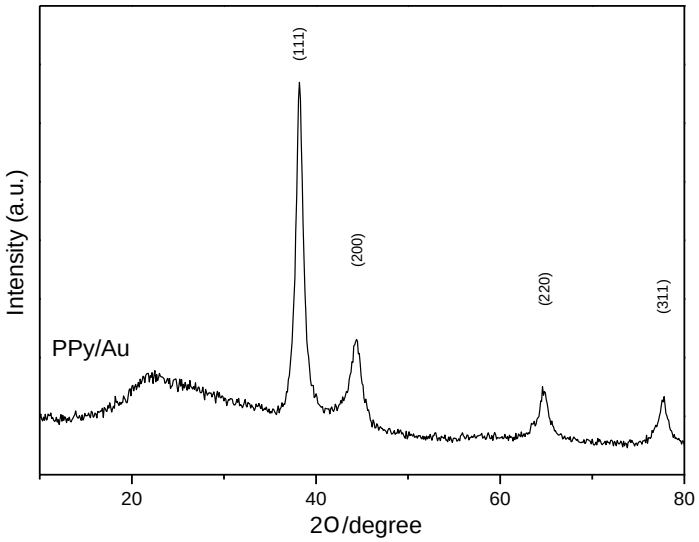

Figure 1.17 : XRD analysis result of PPy- Au

From the above scheme, characteristic peaks are belongs to gold, occupied 38.2^o, 44.3^o, 64.7^o and 77.8^o (JCPDS cart number 101-0056). Besides this, wide peak resulting from polypyrole's amorphous structure was seen between 20 and 30 degree.

1.4.5. Polypyrole-ferrocene-Au nanocomposite

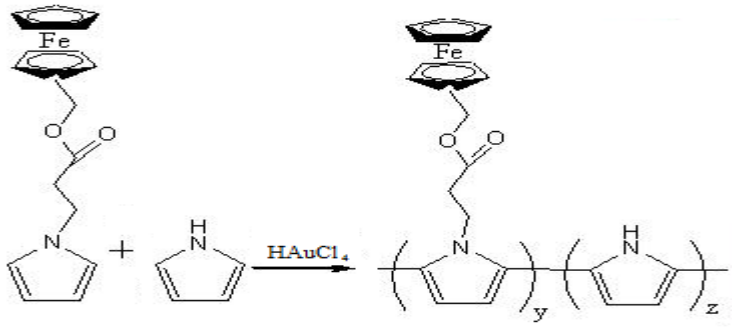

Figure 1.18 : Polypyrole- Ferrocene gold nanocomposite synthesis scheme

Polypyrole-Au ferrocene nanocomposite synthesis was carried out by stirring at 2.5 µl 0.0125M HAuCl4 solution, 2.5 µl 0.0925 M Py-Fc solution and 2.5 µl 0.0925 M Py monomer solution for thirty minute. Then, it was filtered. The nanocomposite was dried in a vacuum oven.

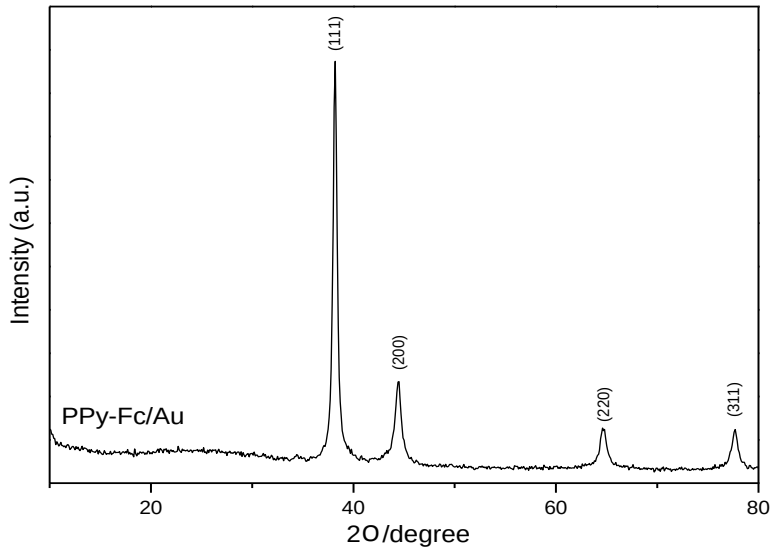

Figure 1.19 : XRD analysis of PPy-Fc-Au nanocomposite

Characteristic peak positions belonging to gold can be observed 38, 44, 64 and 78 degrees. Beside that, a wide peak coming from amorhous structure of PPy, can be observed between 20-30 degre.

1.5. Gases

Chemical and electronic structures of used gases are given in the table below. These data will be useful for us to explain the interactions between the coated material and the gas molecules.

Table 1.2 : Chemical and electronics structures of gas molecules used in the study

Gas	Chemical Structure	3D Structure and Dipole Moment
Carbon dioxide	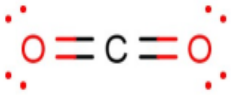	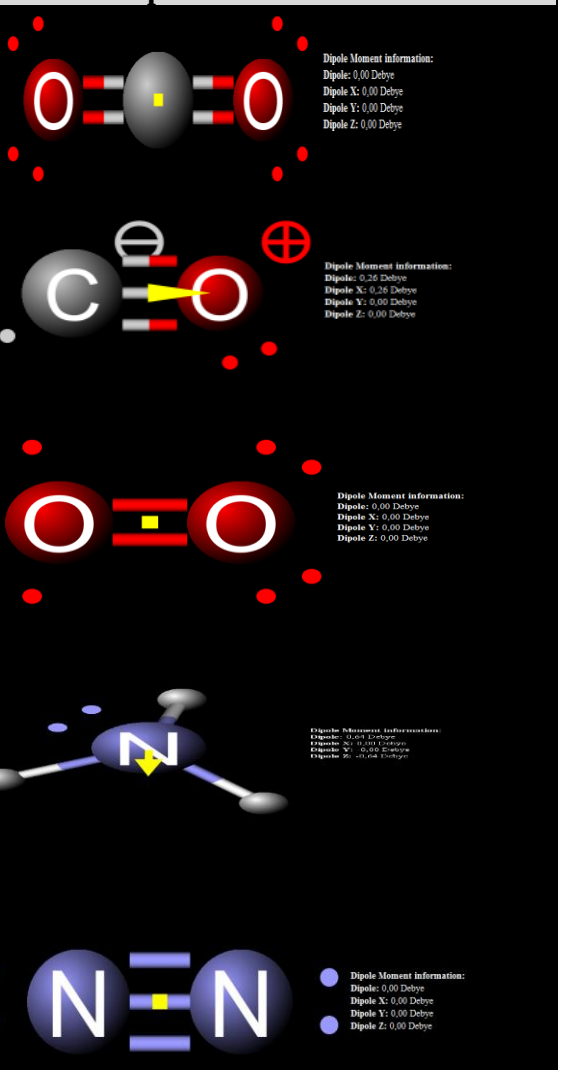
Carbon monoxide		
Oxygen		
Ammonia	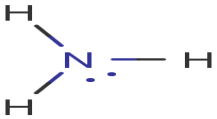	
Nitrogen		

2. EXPERIMENTAL

2.1. Experimental Procedure

The samples were prepared by dispersing 0.1 g of each material in 20 mL dimethylformamide at different vials. These dispersions were stirred for 1 hour on magnetic agitators. Then, dispersions were filtered by 450 nm filter and 50 μL of each dispersion was then drop-cast onto QCM electrodes via a micro-pipette. The electrodes were held for 1 h to promote smooth film formation. After evaporation of the dispersant, (dimethylformamide) a thin film was formed on the electrodes. Each thin film coated electrode was then taken into the gas chamber for gas sorption experiments.

Interdigitated electrodes (IDEs) with 3 μm interdigit separation were fabricated by UV photolithography technique. IDEs were utilized for electrical characterization of the materials. Thin gold wires were used to contact pads on the IDEs via silver paint. After that, thin films of materials were deposited on the IDEs by drop casting. Changes of electrical properties of the deposited thin films due to gas sorption was determined. IDE electrodes were connected to a source meter (Keithly 2636A) for electrical measurements.

The gas measurement chamber was setup in a manner that both QCM and IDE electrode data could be acquired simultaneously. A constant gas flow was sustained through the gas chamber where two electrodes were positioned in a non-intervening way. QCM data was acquired by CHI 440B software, whereas IDE data was acquired by a Lab VIEW program.

Gas measurements were done under three different flow regimes. These are called as periodic, step and linear measurements. A maximum gas flow rate of 500 sccm was used for each of the gas flow regimes during measurements.

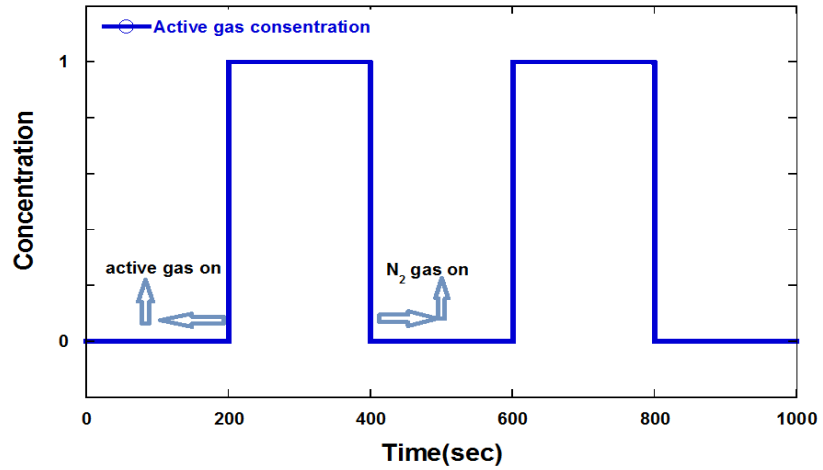

Figure 2.1 : Concentration - time graph of periodic gas flow regime

In periodic measurements, firstly the gas chamber was purged with nitrogen for 200 s to remove any gas molecules adsorbed on the chamber and on the thin film coated electrodes. Next, thin films were exposed to active gases with 100% concentration. This process was repeated twice and the reproducibility of gas sensitivity response for each material was assessed.

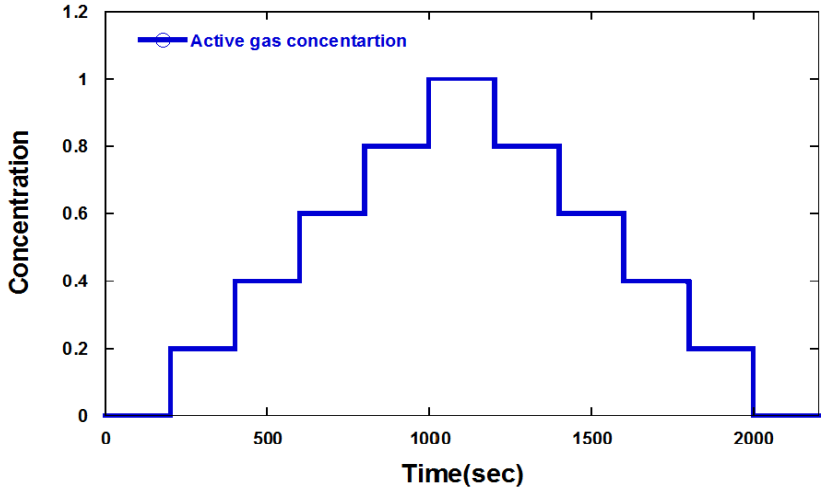

Figure 2.2 : Concentration - time graph of step gas flow regime

In step measurements, active gas flow concentration was varied from 0% to 100% with 20% increments. With this method, gas concentration dependent response of each material was assessed.

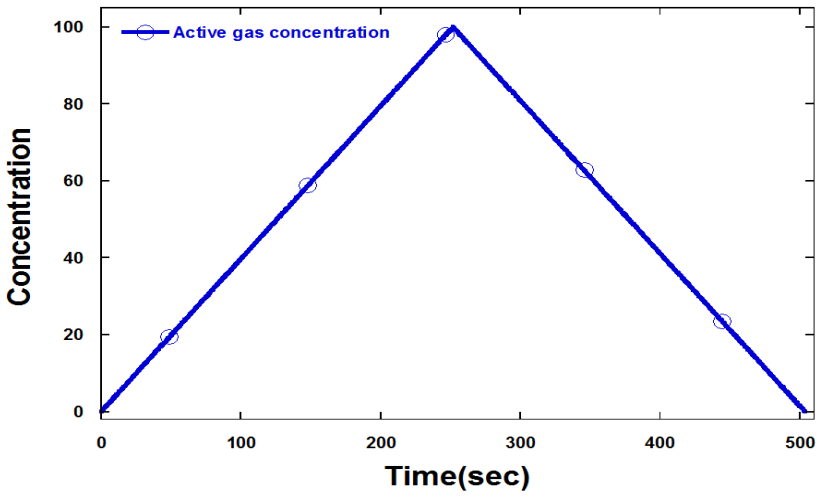

Figure 2.3 : Concentration - time graph of linear gas flow regime

Lastly, in linear measurements, active gas flow concentration was varied from 0% to 100% with 2% increments and sensitivity measurements were carried out under this condition.

2.2. Gas Flow Control Measurement System

The gas measurement setup was composed of three basic sections. The first part was comprised of gas tubes and mass flow meters connected to a mass flow controller unit. A gas flow setpoint was adjusted on the mass flow controller unit and mass flow meters connected to the mass flow controller sustains a continuous and stable flow into the gas chamber within the setpoint ranges. The second part was gas chamber. Being a sealed and airtight cell, this chamber accommodated the QCM electrode and IDE which were coated with thin films of gas sensitive materials. Signals generated by the quartz crystal electrode vibrated via an oscillator were acquired by a frequency counter, whereas signals generated by the IDE on which a constant voltage was applied via a Keithley 2636A source meter was acquired as resistance changes due to gas sorption by the same device. All this setup was controlled by a computer.

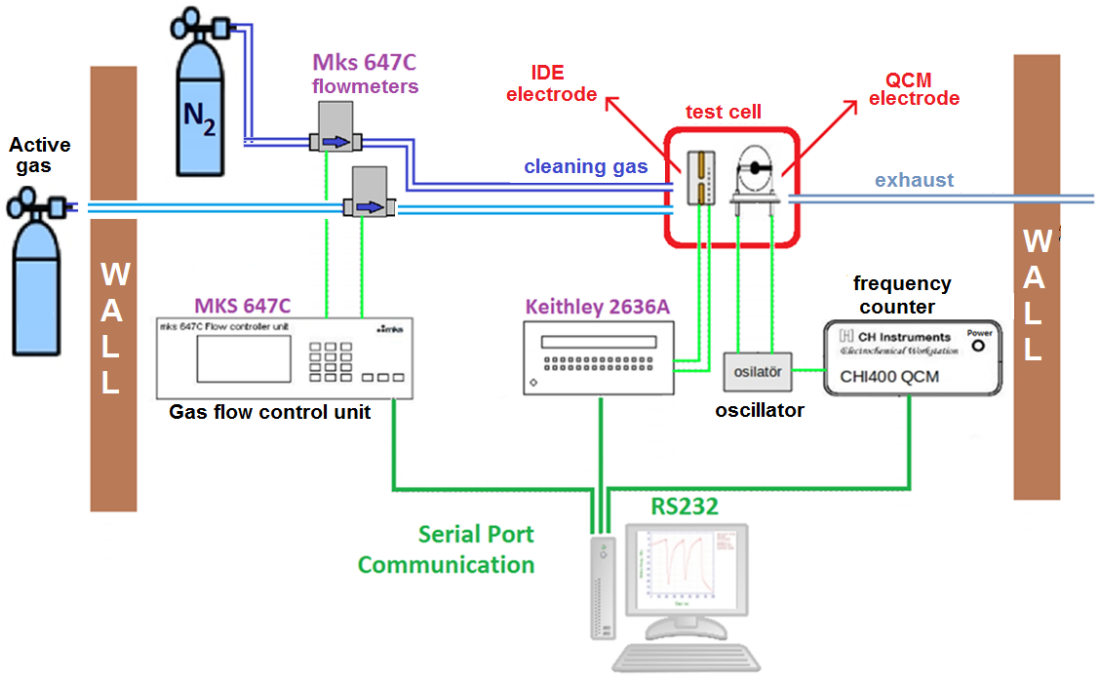

Figure 2.4 : General schematic of the gas flow control measurement system

A CHI 400 model electrochemical analyzer (CH Instruments, Austin, US) was used for QCM measurements. The QCM electrodes (International Crystal Manufacturing Co.) have a diameter of 24 mm, density of 2.684 g/cm3, shear modulus of 2.947 x 1011 g/cm.s2, circular gold coated areas of 0.196 cm2 with 6 mm diameter on both sides. The electrodes can oscillate between 7.995 MHz - 7.950 MHz frequency range with a base frequency of 7.995 MHz. Plugging these data into the Sauerbrey equation yields 1.34 ng of adsorbed mass onto the thin film deposited over the gold coated electrode for 1 Hz of vibrational frequency shift of the QCM electrode.

Six MKS 179A Mass-Flo model mass flow meters (MKS Instruments, US) were used as mass flow meters. Of the six, three had maximum flow rates of 20, 100 and 1000 SCCM (standard cubic centimeter per minute) and were calibrated with CO. The remaining three had maximum flow rates of 100, 1000 and 2000 SCCM and were calibrated with dry air. With these mass flow meters, gas flow rates as precise as 1 SCCM can easily be achieved. ¼ inch pipes were used to transfer gases from gas tanks to flow meters and from flow meters to the gas chamber. The piping was designed in the following way. The six flow meters in the system were divided into two groups. One was reserved for purging gas nitrogen, and the other five were used

for CO, CO2, O2 and other gases. Gas inlets and outlets of the two groups of mass flow controllers were joint within each other to achieve mixed gas flows.
An eight channel MKS 647C model mass flow controller (MKS Instruments, US) was used to control gas flows through the six mass flow meters. The unit has PC connectivity via RS232 interface to switch gas flow on/off, adjust gas flow through selected mass flow meters in determined rates and intervals, and real time flow rate monitoring remotely. It also supported gas calibration with respect to nitrogen via a parameter called GCF (gas correction factor). A purpose-built control software developed via Lab VIEW was used to communicate with the six mass flow controllers through MKS 647C and Keithley 2636A source meter in real time. This enabled simultaneous gas flow control and electrical measurement data acquisition in one software program.

Carbon dioxide, oxygen, nitrogen gases and ammonia, used in the system, were 99.9% pure. Carbon monoxide has been ordered as 10000 ppm diluted with pure N2 gas, Gas outlets were remotely controlled from a PC via electro valves actuated by parallel port commands.

Beside QCM technique to measure gas adsorption kinetics, sensor responces of thin film coated with gas sensitive materials were assessed electrically by IDEs fabricated with lithography techniques.. The area where the gas measurements were carried out was ventilated through a wide window and separated from the rest of the laboratory environment by a PVC lining to prevent potential carbon monoxide in the case of leakage.

The test cell and six mass flow meters were isolated in a metal box to create a Faraday cage that eliminates electromagnetic interference between surrounding field sources and sensitive measurement equipments and expel carbon monoxide which may leak from the gas chamber or connection joints. Additionally, an Industrial Scientific M40 model commercial carbon monoxide gas sensor was used to monitor CO level in the environment in case of CO gas leakage. The whole measurement system could be controlled from a PC remotely by using a remote control software such as Team Viewer.

2.3. Device Fabrication

2.3.1. Photolithography

The most important thing to be successful on the lithography is to get a clean substrate. Ultrasonic bath was used to clean substrates which were glass. Substrates were first dipped in detergent for fifteen minutes then rinsed in distilled water. Then, they were rinsed in acetone, ethanol, iso-propyl alcohol and water for fifteen minutes in ultrasonic cleaner, respectively. Then, pure nitrogen gas was used to dry substrate. All process is depicted in Figure 2.5

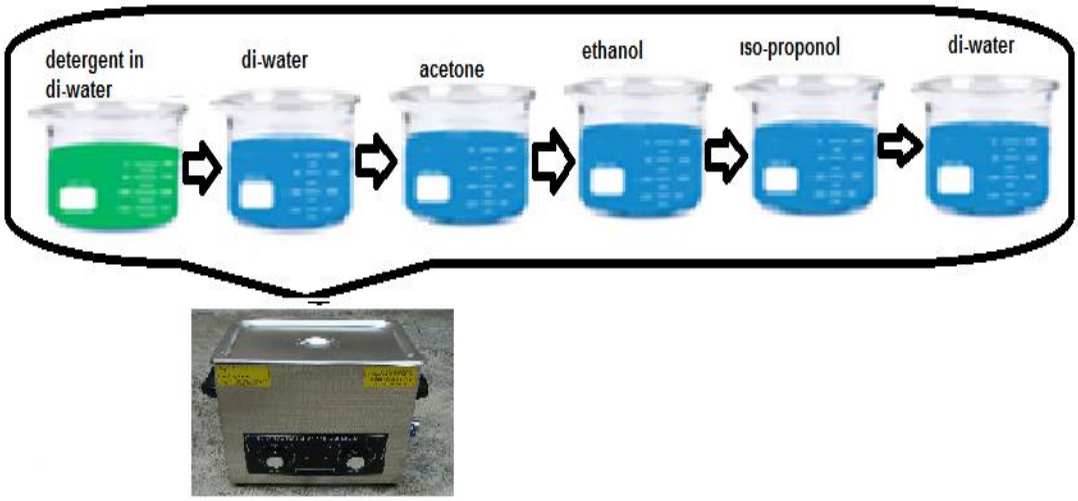

Figure 2.5 : Shematic wiev pad cleaning procedure

Finally, plasma cleaning (with oxygen plasma) process was performed. Plasma cleaning with oxygen plasma removed neutral and technical oils and grease at nanoscale and reduces contamination as seen in Figure 2.6

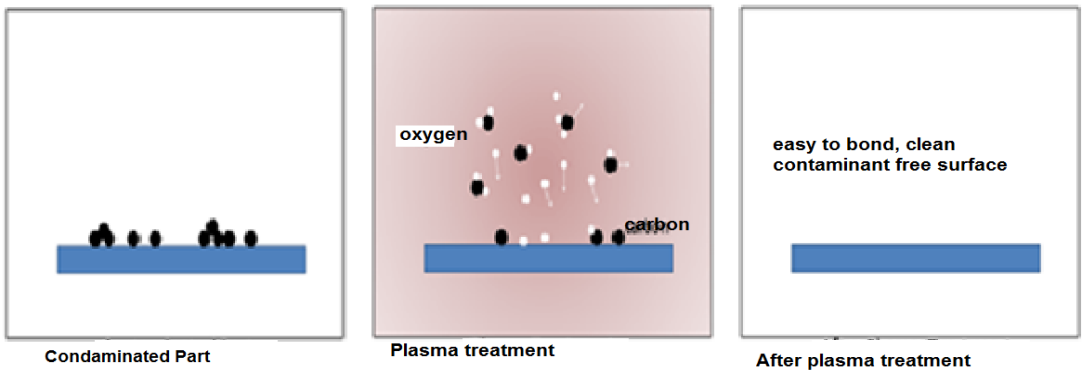

Figure 2.6 : Shematic view of oxygen plasma treatment

Cleaned subtrates were coated with chrome. The thickness of chrome films was chosen around 10 nm. Then, Cr coated sample was coated with gold the thickness of which was around 40 nm. Coating process was carried out by thermal evaporation technique. Here, chrome was used as intermediate later so as to make gold thin film well stick powerfully on substrate. Because, chrome is good sticky material for both glass and gold. At that time, we had double layered thin film on the substrate.

Next step, prepared thin film coated sample was coated by photoresist (AZ1505) acquired microchemical company. This coating process was applied on spin coater for 45 second and the parameter was 4600 rpm. Soft baking process was applied on new photoresist coated sample to get rid of remained liquids on film and to make smooth surface. Sample was heated at 900C for 50 seconds. All thin film so far on sample could be contaminated under the UV light. So, sample was putted under the mask designed specially and was exposed UV light for 3 seconds so as to contaminate unmasked parts on sample. So it was easy to get rid of the contaminated parts on film. After the exposure of UV, the sample was immersed in liquid developer (AZ 726 MIF developer) for 3 minute to etch of the decomposed parts, then it was immediately immersed in distilled water so as not to damage other parts or to stop etching process. Then electrode was dried by nitrogen gas. The prepared film was examined on optical microscope to be sure about good results. After seeing interdjitated electrode, we continued to make experiment with gold etching process. For that, a special solution was prepared. Mixing ratio of solution was 3 HCI: 1 HNO3. Parameters for photoresist developer was used for gold etching process and made dried by nitrogen. Again, optical microscope was used observing the results. As a last part to be etched was chrome film. A special acid solution was used to etch chrome layers. Then we got interdjitated electrode. The distance between all of the fingers were 3 micro meters.

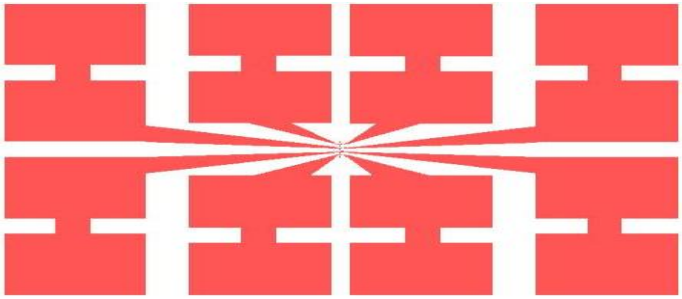

Figure 2.7 : Mask design used to expose positive photoresist

3. RESULT AND DISCUSSION

In this part, gas-sensing properties of the used materials were investigated by quartz crystal microbalance technique. Variation of electrical properties were detected via IDE while interaction thin films annalite and gases.

In order to figure out gas sensor responses of the thin-film coated QCM electrodes, the frequency shift (Δf) of the coated electrode that caused by gas sorption using the CHI 400B time-resolved (EQCM) analyzer should be measured.

Initial resonance frequency (f_0) values of each QCM electrode were recorded in advance for coating. After coating, the resonance frequencies of each coated QCM electrode were recorded again. Then, according to the Sauerbrey equation, after thin-film deposition, the mass of the thin-film material (Δm_0) deposited on the QCM electrode was gained from the frequency difference (Δf_0).

$$\Delta m = 1.34ng \times \Delta f_{\circ} \qquad \textbf{(3.22)}$$

Then we could calculate the mass of gas molecules (Δm) adsorbed on the surface of the thin-film coated electrode after putting the frequency shift (Δf) value of the electrode caused by gas sorption into Sauerbrey equation.

$$\Delta m = 1.34ng \times \Delta f \qquad \textbf{(3.23)}$$

Finally, the ratio between the gas molecules (Δm) that was accumulated on the surface of the thin-film coated QCM electrode and the mass of the thin-film material (Δm_0) deposited on the QCM electrode per mil was determined as the sensor response (S) of each sensor material to CO, CO_2, O_2 and NH_3.

$$S = \frac{\Delta m}{\Delta m_{\circ}} \times 1000 \qquad \textbf{(3.24)}$$

The frequency dependant form of the sensor response relation was obtained after substituting Δm and Δm_0 with Δf and Δf_0 respectively.

$$S = \frac{\Delta f}{\Delta f_{\circ}} \times 1000 \qquad \textbf{(3.25)}$$

On the other hand, using the Keithley 2636A SYSTEM Source Meter under a current value for about 1.0000 mA to measure the changes in resistance through the thin-film coating would determine the responses from the folded electrodes.

There was also another way to determine the sensor response (S) of each sensor material to CO, CO_2, O_2 and NH_3. It was by calculating the ratio of the resistivity R of the thin-film coated IDE electrode under active gas (N_2) mixture atmosphere to the resistivity R_0 of the IDE electrode under pure N_2 atmosphere.

$$S = \frac{|R - R_{\circ}|}{R_{\circ}} 100 \qquad \textbf{(3.26)}$$

3.1. Quartz Crystal Microbalance Results

Gold-doped polypyrrole based materials gas sorption properties against CO, CO_2, O_2 and NH_3 were investigated by QCM teqnique. Raw data graphs can be seen in this part. Their sensor responses were calculated according to the experimental results.

3.1.1. Periodic measurements results

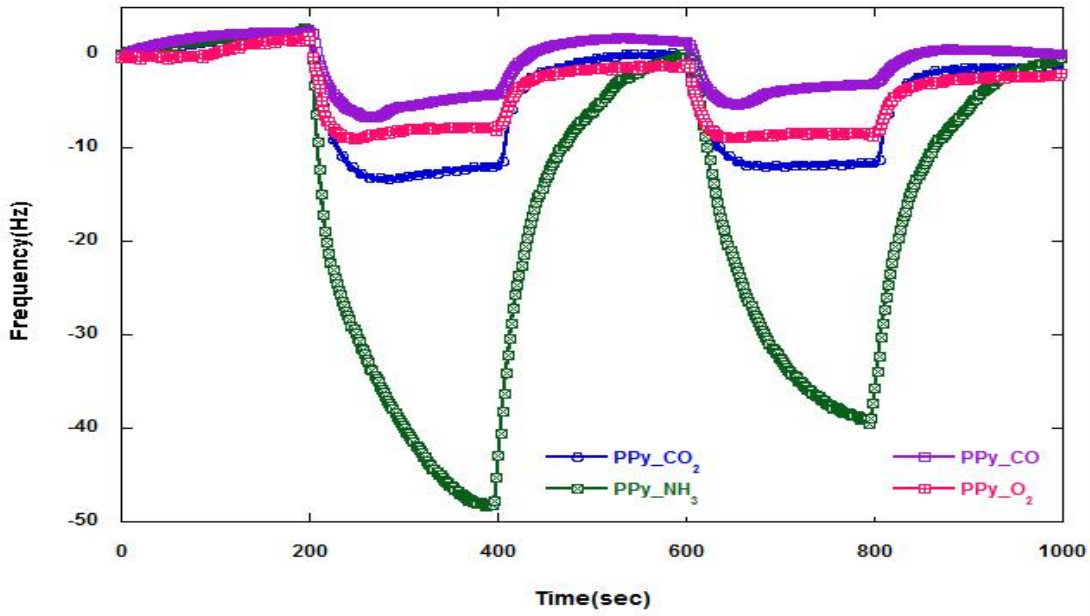

Figure 3.1 : Gas responses of PPy thin-film coatings against CO, CO_2, O_2 and NH_3 under periodic gas flow regime

Figure 3.1 shows raw datas graphs of PPy thin-film coatings against CO, CO_2, O_2 and NH_3 under periodic gas flow regime. Maximum response, far ahead of other used gases, was observed againts NH_3 gas. That is resulted from hydrogen bonding and dipole-dipole interractions as it was stated in the literature [100]. Active side of ammonia is two lone-paired electrons that physically interact with polypyrrole active sides[101]. For PPy, the sensor responce is directly proportional to molecular weight of gases because the same film was used with same number of active sides. As it is understood from the graph, maximum response of the PPy sensor at second cycle decreases specifically for ammonia. This could be the reason of decreased number of active sites on the thin film. Between PPy and CO, weak hydrogen boding is expected which result in higher sensor response. However, lowest response was observed to CO gas. CO_2 molecules also form weak bonds with π-electrons of PPy [102]. O_2 is also expected to form weak hydrogen bond with PPy. Nevertheless, for CO, CO_2, O_2, weak bonds was not so effective for sensing ability of PPy in this measurements output.

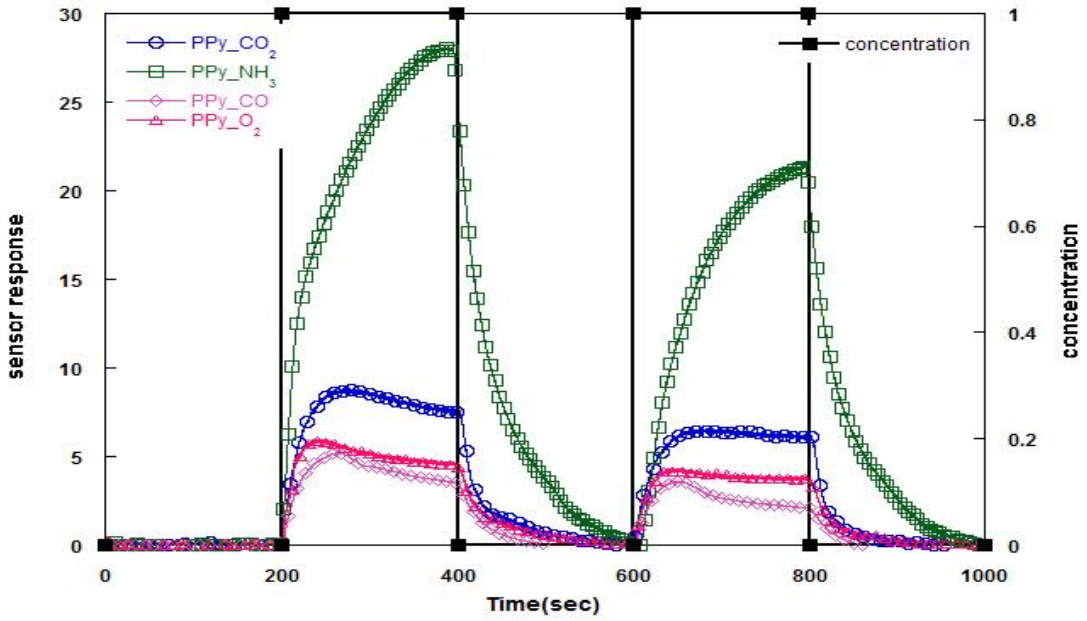

Figure 3.2 : Gas responses of PPy thin-film coatings against CO, CO_2, O_2 and NH_3 under periodic gas flow regime

Figure 3.2 shows the response of polypyrrole to CO, CO_2, O_2 and NH_3 under the periodic gas flow regime. Here, sensitivity calculations were performed. Response order of the PPy-coated thin film is same as raw data graps in Figure 3.1. Because all experiment were conducted with same thin film coated QCM electrode and for all gases treatment parameters were same.

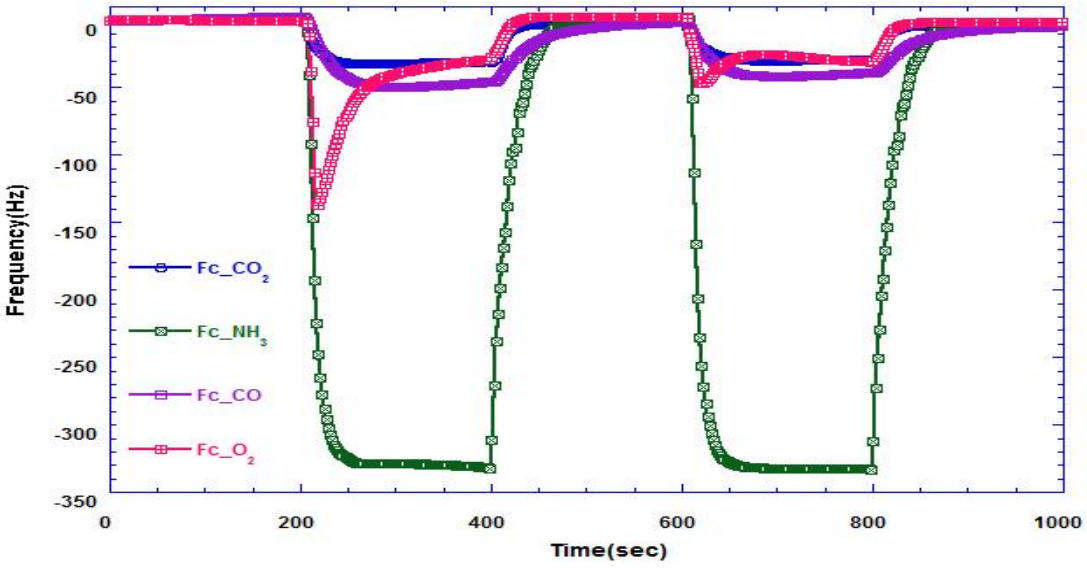

Figure 3.3 : Gas responses of Fc thin-film coatings against CO, CO_2, O_2 and NH_3 under periodic gas flow regime.

Figure 3.3 shows raw datas graphs of Fc thin-film coatings against CO, CO_2, O_2 and NH_3 under periodic gas flow regime. Comparing with the magnitude of sensor response of Fc NH_3 is highter than CO, O_2, and CO_2. Formation of H bond is in charge of the response in case of ammonia whereas formation of weak H bond brings about response for other gases. Fe atom has specific affinity to CO gas and therefore CO become prominent in response intensity compare to O_2 and CO_2. Fe is active side in Fc and plays main role in interaction of gases with Fc, but Wander-Waals interactions could happen in Cp. Moreover, the reason of strange response of O_2 in the first cycle could be treatment of same film with other gas in previous experiment or remaining of O_2 gas on the film surface which could result in decrease in activity against O_2 although not seen in qcm. However, the film surface recovered itself in second cycle and showed the same response (it is not reported here)

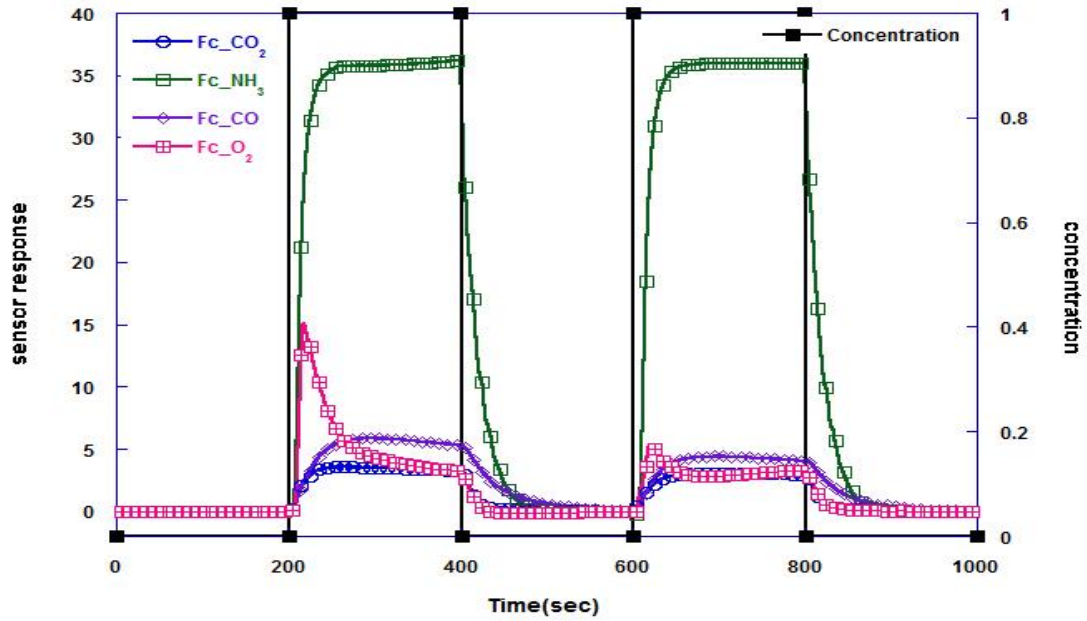

Figure 3.4 : Gas responses of Fc thin-film coatings against CO, CO_2, O_2 and NH_3 under periodic gas flow regime.

Figure 3.4 shows the response of ferrocene to CO, CO_2, O_2 and NH_3 under the periodic gas flow regime. Here, sensor response calculations were performed.

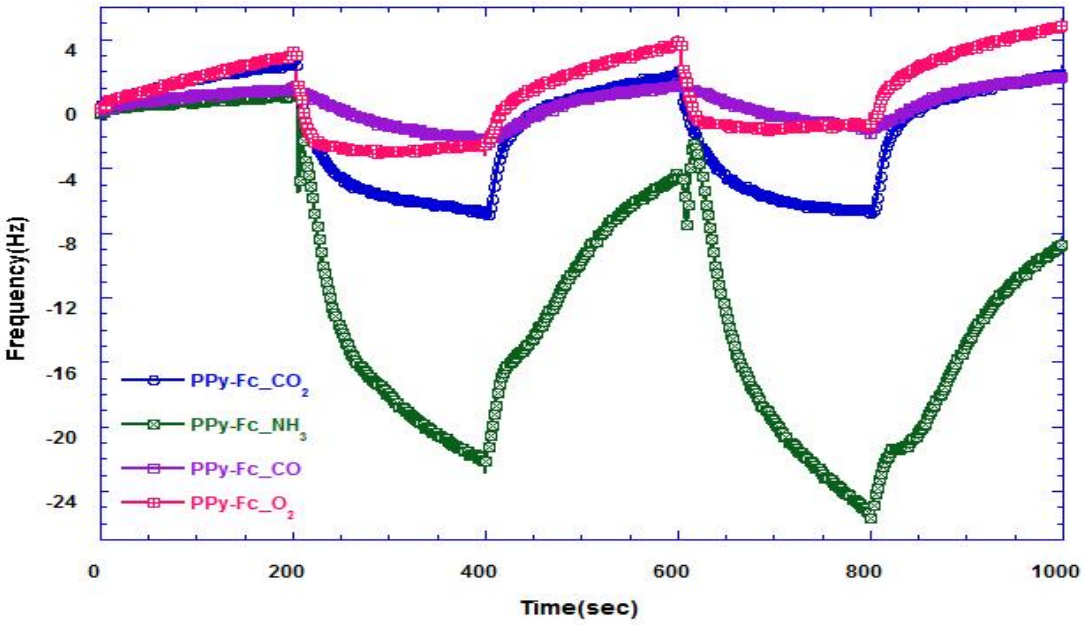

Figure 3.5 : Gas responses of PPy-Fc thin-film coatings against CO, CO_2, O_2 and NH_3 under periodic gas flow regime.

Figure 3.5 shows the raw data graphs of polypyrrole-ferrocene to CO, CO_2, O_2 and NH_3 under the periodic gas flow regime. The biggest response of PPy-Fc against used gases was seen in ammonia due to H-bonds. The response against other gases occurred owing to weak H-bonds and this response is directly proportional to their molecular weight. The response times of material against gases are long as well as do not reach saturation point. This is thought to be because of steric effect. Cp in conjugated Fc physically blocked to active sides in PPy and prevented easy access of gases. Consequently, response time increased and the film surface was not saturated. However, O_2 saturated the film surface. Molecular size of O_2 is bigger than molecular size of CO, but smaller than other gases. It is thought that material is selective to CO since CO is more polar than O_2.

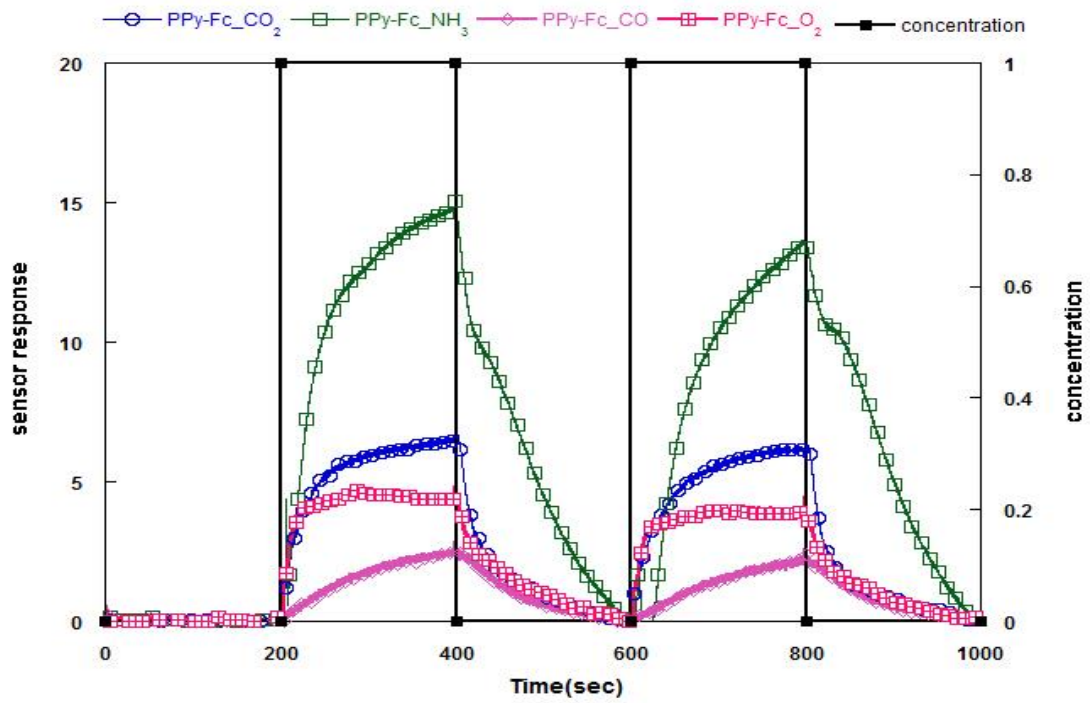

Figure 3.6 : Gas responses of PPy-Fc thin-film coatings against CO, CO_2, O_2 and NH_3 under periodic gas flow regime.

Figure 3.6 shows the response of Polypyrrole-Ferrocene to CO, CO_2, O_2 and NH_3 under the periodic gas flow regime. Here, sensor response calculations were performed. Second cycle of ammonia responded slightly lower than the first. That is a result of decreasing trend of ammonia.

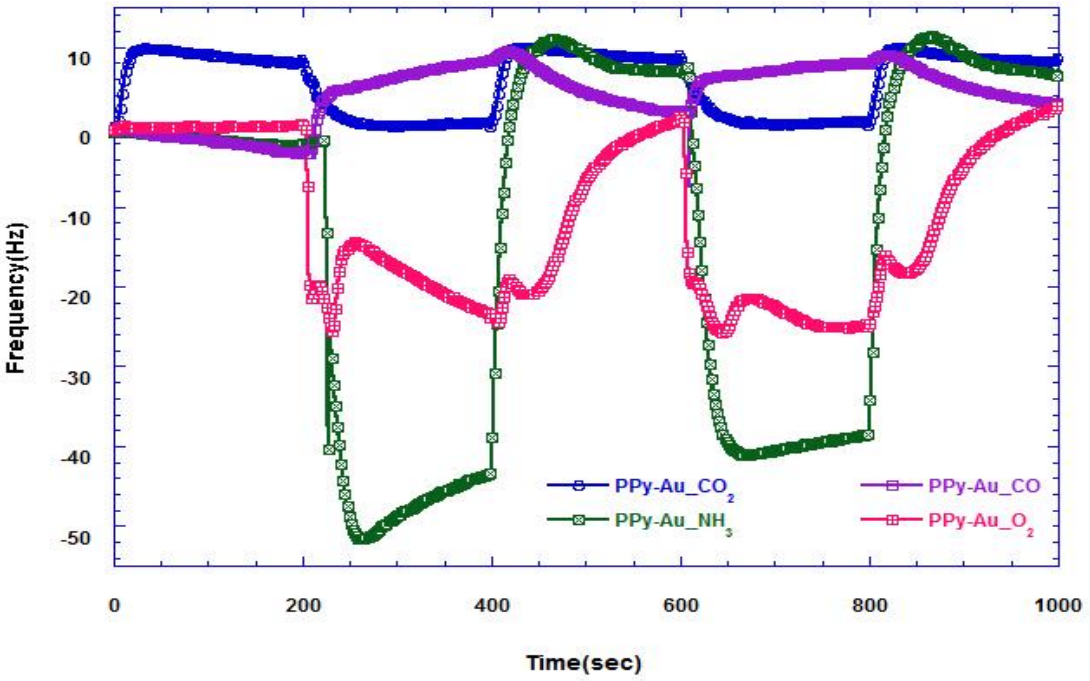

Figure 3.7 : Gas responses of PPy-Au thin-film coatings against CO, CO_2, O_2 and NH_3 under periodic gas flow regime.

Figure 3.7 shows the raw data graphs of polypyrrole-Gold to CO, CO_2, O_2 and NH_3 under the periodic gas flow regime. PPy-Au nanocomposites film reached saturation against NH_3 in much shorter time compared to O_2 and CO_2. Cleavage of NH_3 and CO_2 easily occurred during the treatment of surface with N_2. Therefore, it can be considered that surface area of film increased after gold doping. Nevertheless, thin film gave peculiar response to CO. It is expected an interaction with weak H-bonds between adsorbed molecules to be able to give positive QCM response, yet this is impossible for CO. The reason of strange response against O_2 gas might be treatment of surface against O_2 gas after the treatment against CO. It is pondered that remaining CO molecules on the film surface could bring about positive qcm effect. For CO_2, the higher frequency compare to other gas at first 200 seconds may be possibly due to not fully cleaned film.

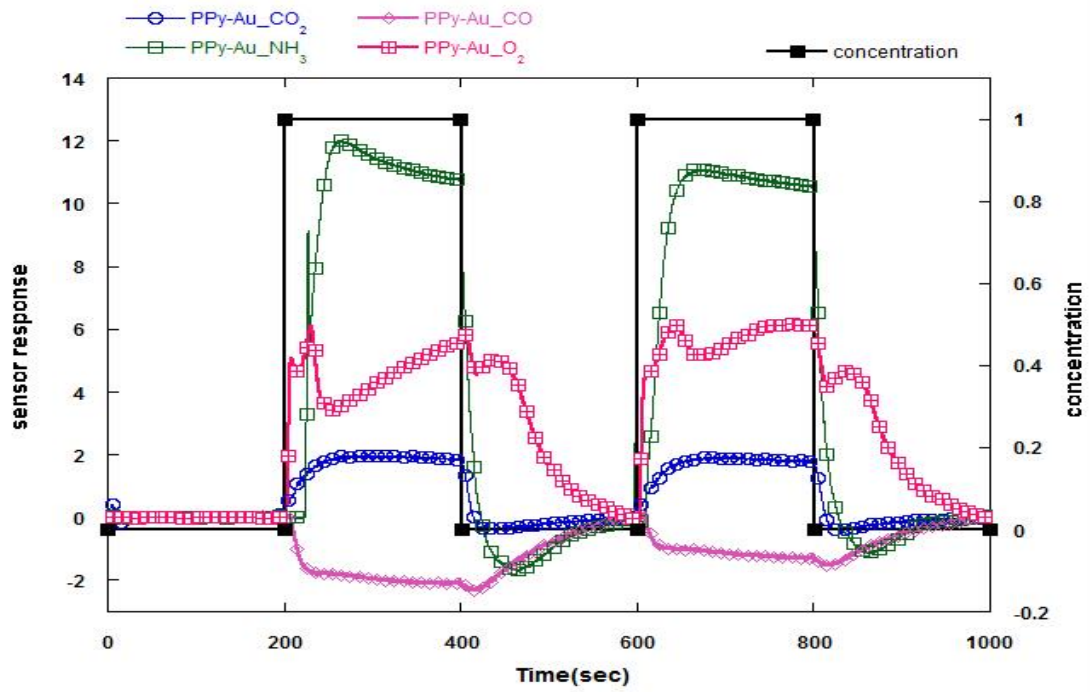

Figure 3.8 : Gas responses of PPy-Au thin-film coatings against CO, CO_2, O_2 and NH_3 under periodic gas flow regime.

Figure 3.8 shows the sensor response of Polypyrrole-gold thin-film coating against CO, CO_2, O_2 and NH_3 under the periodic gas flow regime.

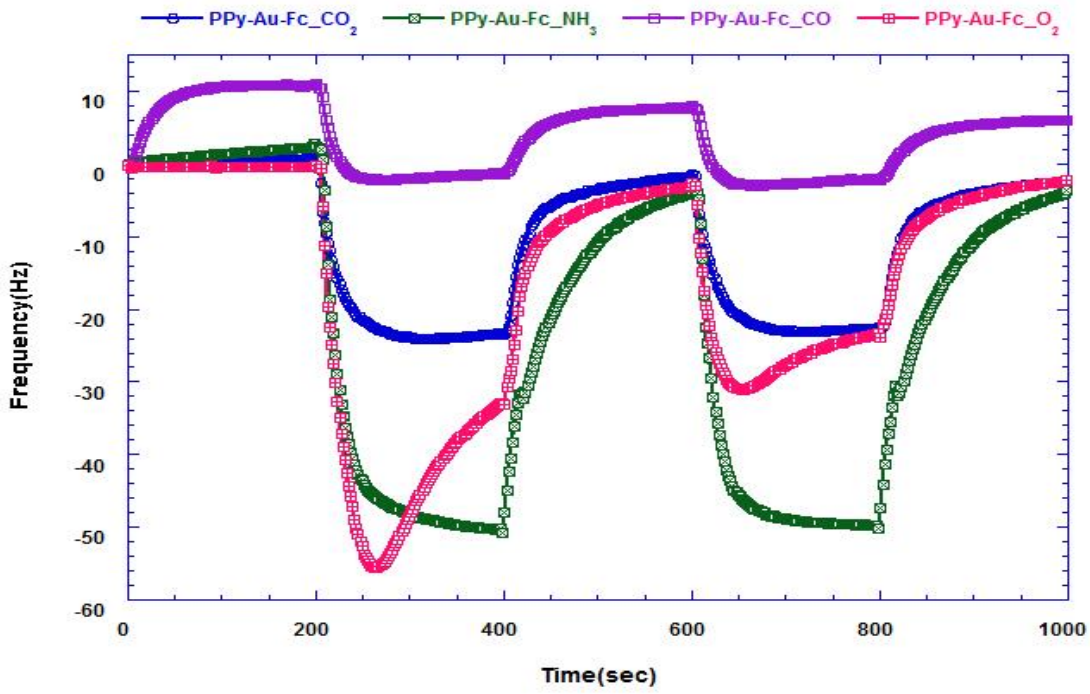

Figure 3.9 : Gas responses of PPy-Au-Fc thin-film coatings against CO, CO_2, O_2 and NH_3 under periodic gas flow regime.

Figure 3.9 shows the raw data graphs of Polypyrrole-Gold-Ferrocene against CO, CO_2, O_2 and NH_3 under the periodic gas flow regime. Response time of PPy-Fc-Au nanocomposite thin film against gases was short which means the film was so active to gases. In the first period of 200 second, the increase in the frequency proved that there were adsorbed gas molecules on the film which also meant that the film was quite active to gases. The reason why this film was so active might be because of the increase in the surface area depending on the Au doping. The reason, why the film showed higher affinity towards O_2 than NH_3 and positive QCM was seen, might be because of conjugation of Fc to PPy as similar behavior seen on Fc. Similarly, it was considered that CO measurement which was done in advance might have caused higher response to O_2. CO graph depicts that at the end of the first desorption period the frequency shift was 10 Hz, while it was around 5 Hz at the last part of the second desorption period which proved that there was still CO molecules on the surface of the film. The porosity of the film might be the reason of the poor cleaning of the surface. Similarly, looking at the second cycle, it is seen that the adsorbed molecules was partially removed from the surface of the film for all gases. If we sort the sensor responses from largest to smallest for the second period, the sequence will be as NH_3, O_2, CO_2 and CO. Due to strong hydrogen binding, more affinity towards NH_3 was observed. However, the sequence of the sensor response for other gases was not proportional to the molar mass of the molecules but still it was considered that if the period had been kept shorter, this assumption might have hold since the response to O2, which spoiled the sequence, was gradually decreasing.

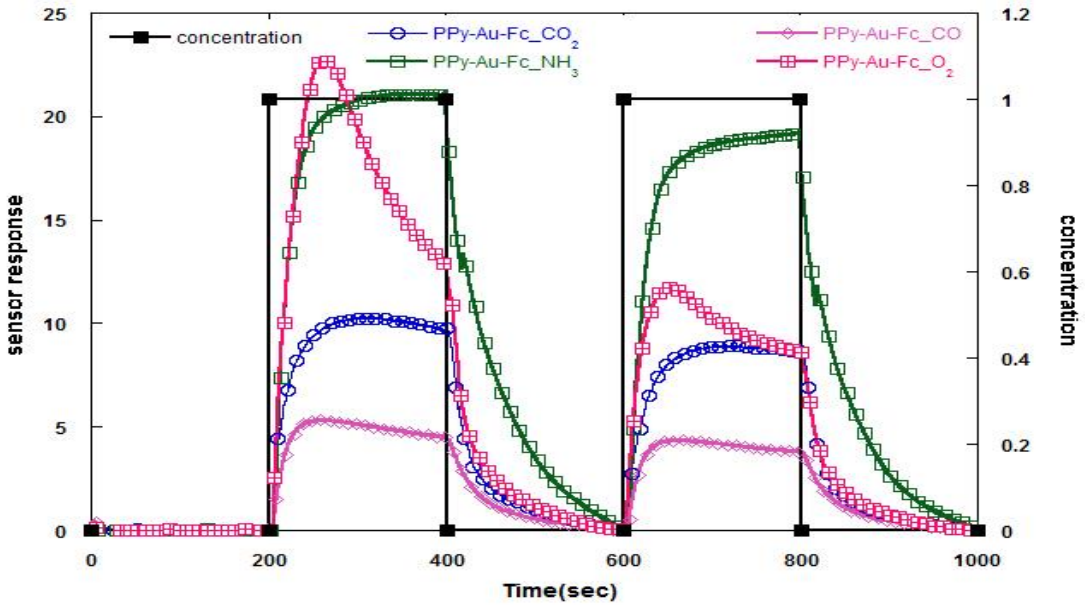

Figure 3.10 : Gas responses of PPy-Au-Fc thin-film coatings against CO, CO_2, O_2 and NH_3 under periodic gas flow regime.

Figure 3.10 shows the response of Ppy-Au-Fc thin-film coating against CO, CO_2, O_2 and NH_3 under the periodic gas flow regime. Sensor response calculations were conducted.

Table 3.1 : Maximum sensor response values of all conducted materials

Materials	**Maximum sensor response value (‰)**			
	CO	**CO_2**	**NH_3**	**O_2**
Polypyrrole (PPy)	**5.19**	**8.83**	**28.19**	**5.96**
Ferrocene (Fc)	**5.87**	**3.56**	**36.35**	**5.11**
Polypyrrole-Ferrocene (PPy-Fc)	**2.81**	**6.80**	**50.83**	**4.79**
Polypyrrole-Gold-Ferrocene (PPy-Au-Fc)	**5.35**	**10.33**	**21.20**	**12.74**
Polypyrrole-Gold (PPy-Au)	**2.15(positive qcm)**	**2.02**	**12.01**	**6.08**

An optimization was performed to eliminate the effect of mass of the film which is coated on QCM electrode. This result was calculated as sensor response above. The F_0 value is the frequency shift between coated and uncoated QCM electrode. The

reason why the mass of the coated film is important is because this value should not exceed the working range of the QCM electrode. Therefore, the property of the film is related to the molar mass of the used material. The most important property of the used polymer for gas adsorption process is that the molecules have active sites which have impact on the interaction between film and active gas. These bindings between the active sites and adsorption gases involve hydrogen bonding or Van der Waals interaction. From the point of this view, it can be concluded that the amount of the active sites are quite important for adsorption process.

The sensor response was optimized according to calculation given above; however, the change in the surface area and porosity due to gold doping and Fc conjugation was not taken into account. The most important part , however, is that the parameters which are directly related with the sensor response such as the change in the mass of the film by doping or conjugation, the relation between the amount of the active sites due to doping and conjugation, was not investigated at first glance. If it is considered as a monomer, there should not be any change in the amount of the active sites, surface area may have increased, though. In addition to this, the mass of the prepared nanocomposite film will be increased since the molecular weight of the pyrrole is 67.09 g/mol while the molar mass of the gold is 196.96 g/mol. However, there will not be any decrease in the amount of the active sites after conjugation with Fc. In Fc, Fe atom is the active site and it is expected to interact with gases but there is still small possibility to see Van der Waals interaction due to Cp. There are two active sites one of which is coming from Fc and the other one is coming from pyrrole. The increase in the amount of the active sites may require an increase in the sensor response but there may not be any difference unless it is considered with the mass of coated film since the molar mass of the Fc is 186.04 g/mol while the molar mass of the pyrrole is 67.09 g/mol.

While the sensor response of PPy to CO is 5.19, it is 2.15 for PPy-Au nanocomposite. Here, it is rather difficult to compare the results reasonably due to positive QCM response.

The sensor responses of PPy and PPy-Au to CO_2 are 8.83 and 2.02, respectively. Normally, an increase in the sensor response was expected depending on increase in

the surface area; however, PPy-Au nanocomposite showed poor response due to the fact that molar mass of the gold is high enough.

A very low response was seen for NH3 due to same reason given above. If the responses of PPy and PPy-Au were compared, it could be said that there was an increase in the surface area due to gold doping because there was a decrease in response time as seen in PPy-Au graph. As soon as active gas was sent, the sensor film became saturated in a short time. If the slope of this part is investigated it will be seen that the response time is quite small which is due to high slope.

Although the response to O_2 was as expected for PPy, higher sensor response was observed for PPy-Au nanocomposite contrary to expectation which might be due to the fact that this experiment was performed just after CO experiment.

It is expected that PPy conjugation with Fc increase gas sensor response to various gases. Au doping to polymers increase surface area of the thin film that's why response time decrease against the gases.

Sensor responses of PPy, Fc and PPy-Fc were respectively 5.18, 5.87 and 2.81 ‰ against CO. It is usually expected that gas sensor response of PPy-Fc will be between less sensitive one and the sum of the sensor responses of PPy and Fc. If the PPy-Fc was exposed to the CO gas for long time, sensor response might have been increased. Because PPy-Fc did not reach saturation point against the CO. Steric effect was observed on the PPy-Fc thin film against the CO. Gold doping to PPy-Fc increased the sensor response to the CO. İncreasing of thin film surface area might cause increasing the sensor response.

PPy response to CO_2 was 8.83 ‰ and Fc response to the CO_2 was 3.56 ‰. PPy-Fc sensor response was 6.8 ‰. If the PPy-Fc was exposed to CO_2 gas for long time, sensor response might have been increased. Because PPy-Fc did not reach saturation level against the CO_2. Steric effect was observed on the PPy-Fc thin film against the CO_2. Gold doping to PPy-Fc increased sensor response, reaching 10.33 ‰, to the CO_2. Gold doping might increase surface area of the thin film.

Sensor responses of PPy and Fc against the NH_3 was respectively 28.19 and 36.35 ‰. Conjugation of PPy with Fc increased the sensor response, reaching 50.83 ‰,

against the NH3. Steric effect was observed on the PPy-Fc thin film against the NH3. Gold doping PPy-Fc decreased sensor response. Decreasing sensor response of PPy-Fc-Au nanocomposite might be result of increasing mass of thin film although, surface area might be increased.

Sensor responses of PPy and Fc was respectively 5.96 and 5.11 ‰. PPy-Fc sensor response, was 4.79 ‰, was close to their sensor response values. For sensor responses of PPy-Fc against O_2 reached saturation level although the sensor response didn't reached against the other gases. Molecular sizes might have played an important role in such a sensor response. Ammonia size is the biggest in all gases, than the second is CO_2's size. CO has the smallest size but its size is close to O_2. PPy-Fc sensor response against CO didn't reach saturation level although the response against O_2 reached saturation level. This distinction between CO and O_2 might be based on polarity of molecules. As a result of increasing thin film surface area, sensor response against O_2 increased by gold doping to PPy-Fc

All in all, PPy-Fc sensor responses increased against CO, CO_2, O_2, making weak H bond, by gold doping

3.1.2. Step measurements results

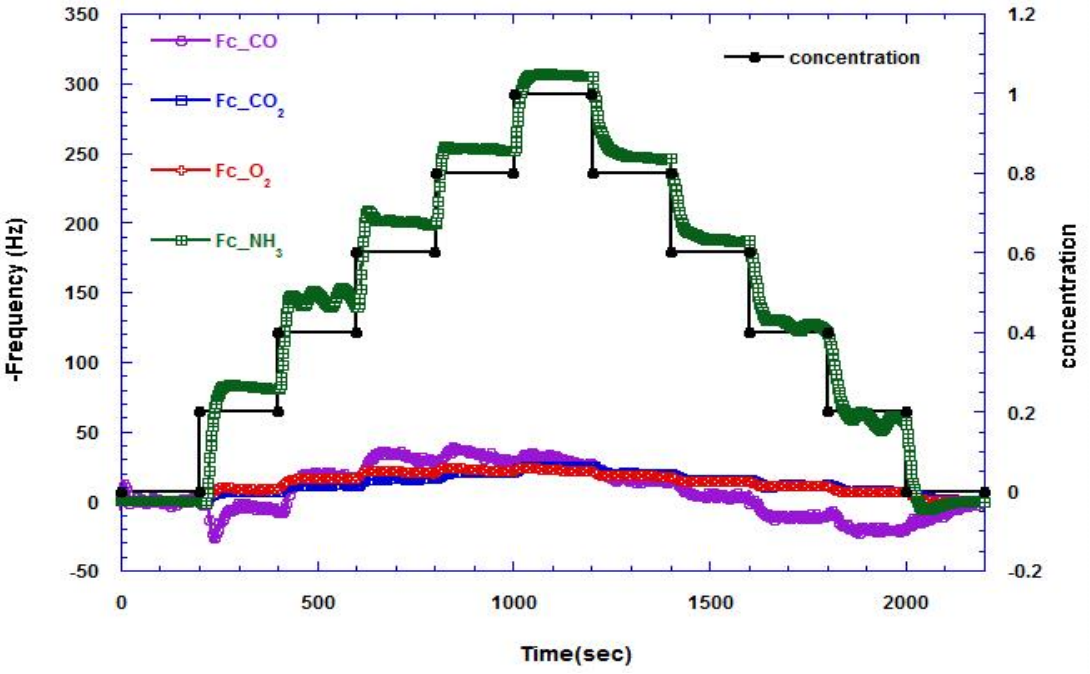

Figure 3.11 : Gas responses of Fc thin-film coatings against CO, CO_2, O_2 and NH_3 under step gas flow regime.

Figure 3.11 shows gas responses of Fc thin-film coatings against CO, CO_2, O_2 and NH_3 under step gas flow regime. Begining of 0.2 concentration step, a non-linear response was observed. Nevertheless, in the next steps non-linear response turned into a linear response. At initial low concentration, multi layer adsorption of CO molecules might cause non-linear response. However, by increasing gas concentrations, a gradual decrease in multi-layer surface coverage that ultimately reached equilibrium at the maximum gas concentration was observed. This effect can be explained by the electrostatic repulsion of gas molecules to the multilayer adsorbed molecules on the surface.

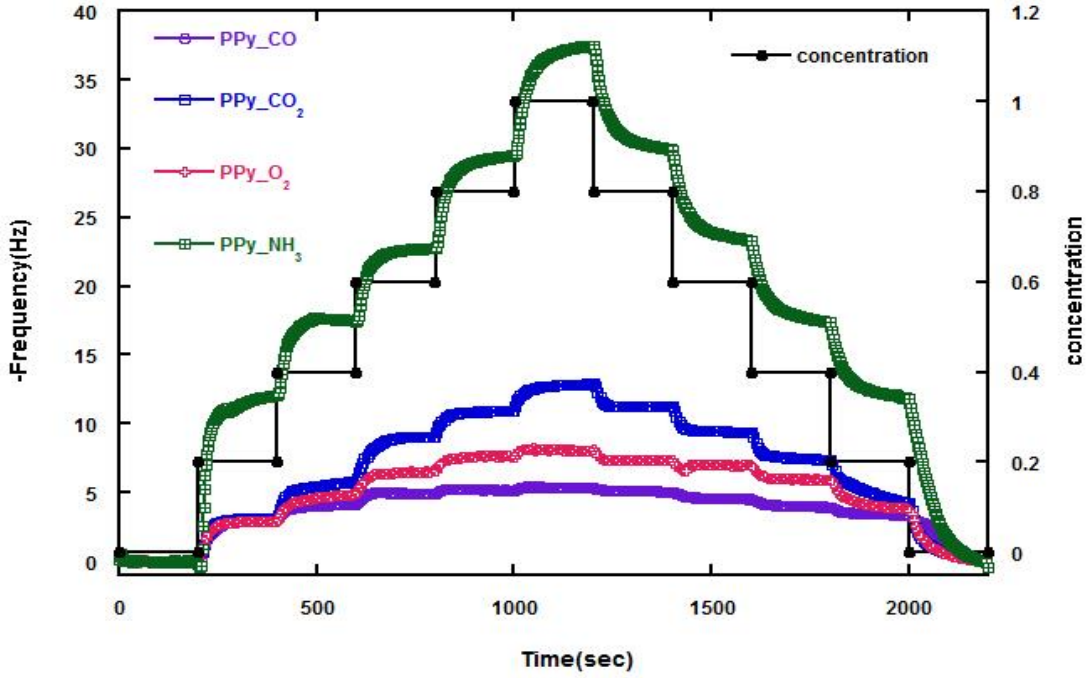

Figure 3.12 : Gas responses of PPy thin-film coatings against CO, CO_2, O_2 and NH_3 under step gas flow regime.

Figure 3.12 shows gas responses of PPy thin-film coatings against CO, CO_2, O_2 and NH_3 under step gas flow regime. Highest response was shown to NH_3. All of the concentration changes can be observed from the graphs.

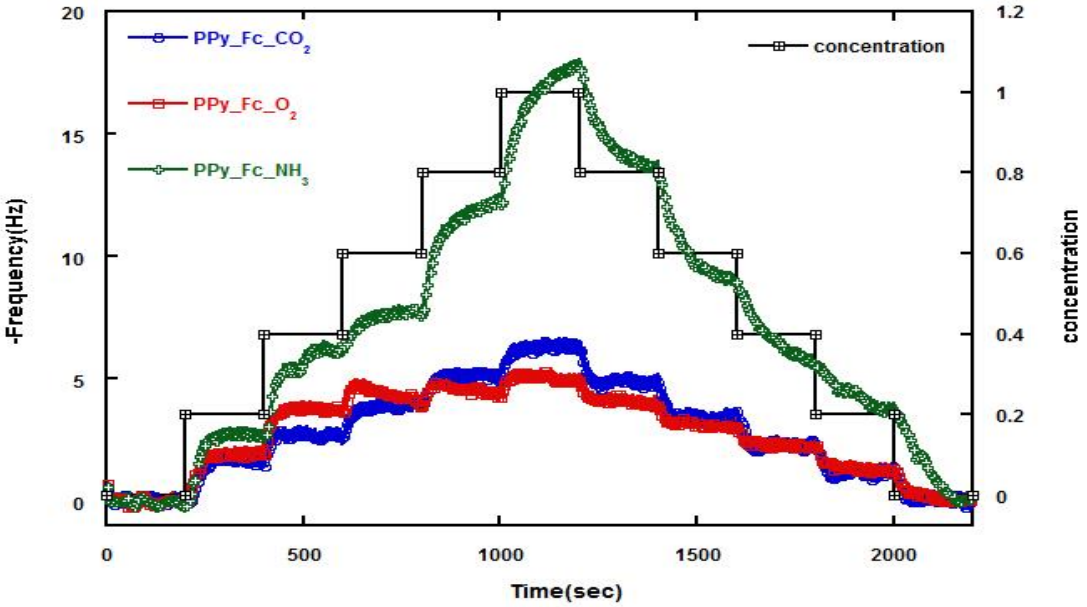

Figure 3.13 : Gas responses of PPy-Fc thin-film coatings against CO_2, O_2 and NH_3 under step gas flow regime.

Figure 3.13 Gas responses of PPy-Fc thin-film coatings against CO, CO_2, O_2 and NH_3 under step gas flow regime. For PPy-Fc, CO data cannot be put into the graph because measurements' outputs were not meaningful. Each concentration step can be observed.

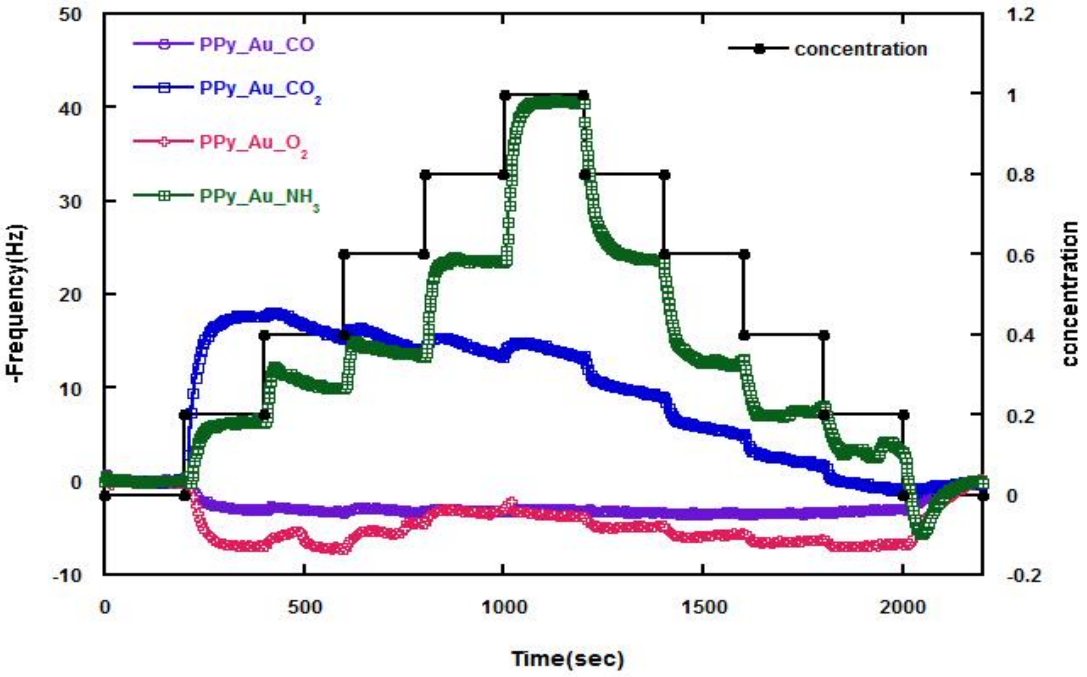

Figure 3.14 : Gas responses of PPy-Au thin-film coatings against CO, CO_2, O_2 and NH_3 under step gas flow regime.

Figure 3.14 shows gas responses of PPy-Au thin-film coatings against CO, CO_2, O_2 and NH_3 under step gas flow regime. A prominent non-linear QCM response was observed against O_2 and CO. At the initial low concentrations, a rapid coverage of the film surface, accompanying with multilayer adsorption of O_2 and CO molecules was observed. However, by increasing gas concentrations, a step-by-step decrease in multi-layer surface coverage that ultimately reached equilibrium at the maximum gas concentration was observed. Electrostatic repulsion of gas molecules to the multilayer adsorbed molecules on the surface might cause this effect. While increasing the partial pressures of the gases in the gas mixture, O_2 and CO molecules impacting on the surface imposes forces higher in magnitude than the forces binding multilayer adsorbed O_2 and CO molecules to the surface, thus removing multilayer adsorbed molecules from the surface, resulting in a gradual decrease from the initial non-linearity. This action clearly shows the prominent characteristics of a self-limiting reaction, since, as the O_2 and CO partial pressures decrease, multilayer adsorption is promoted again, restoring the initial non-linear effect.

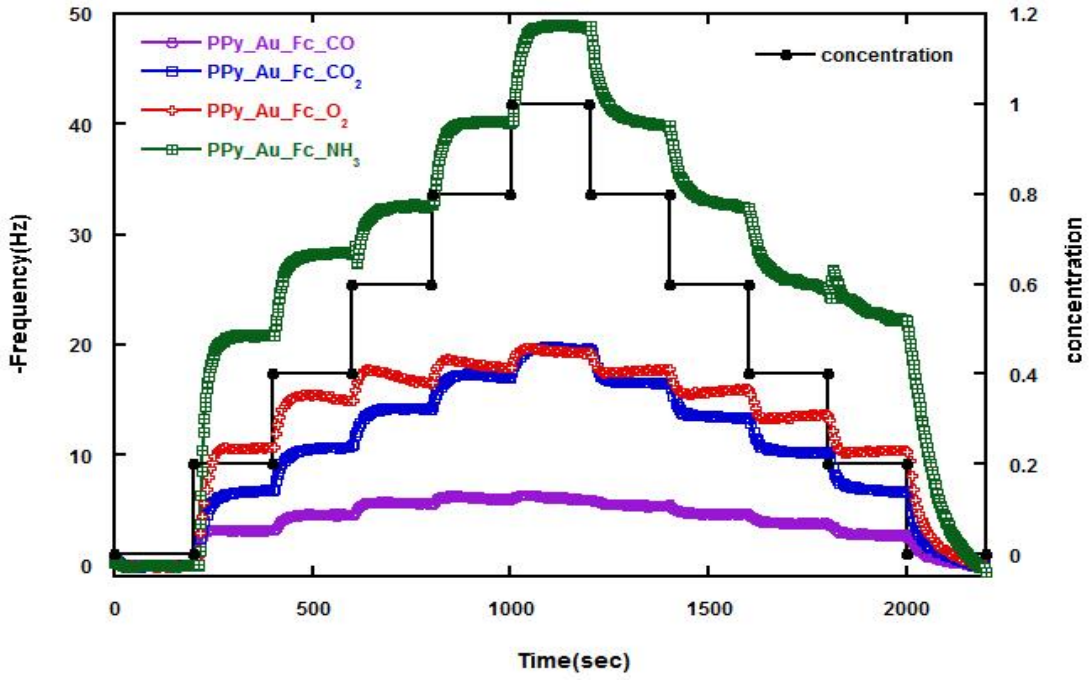

Figure 3.15 : Gas responses of PPy-Au-Fc thin-film coatings against CO, CO_2, O_2 and NH_3 under step gas flow regime.

Figure 3.15 shows gas responses of PPy-Au-Fc thin-film coatings against CO, CO_2, O_2 and NH_3 under step gas flow regime.

3.1.3. Lineer measurements results

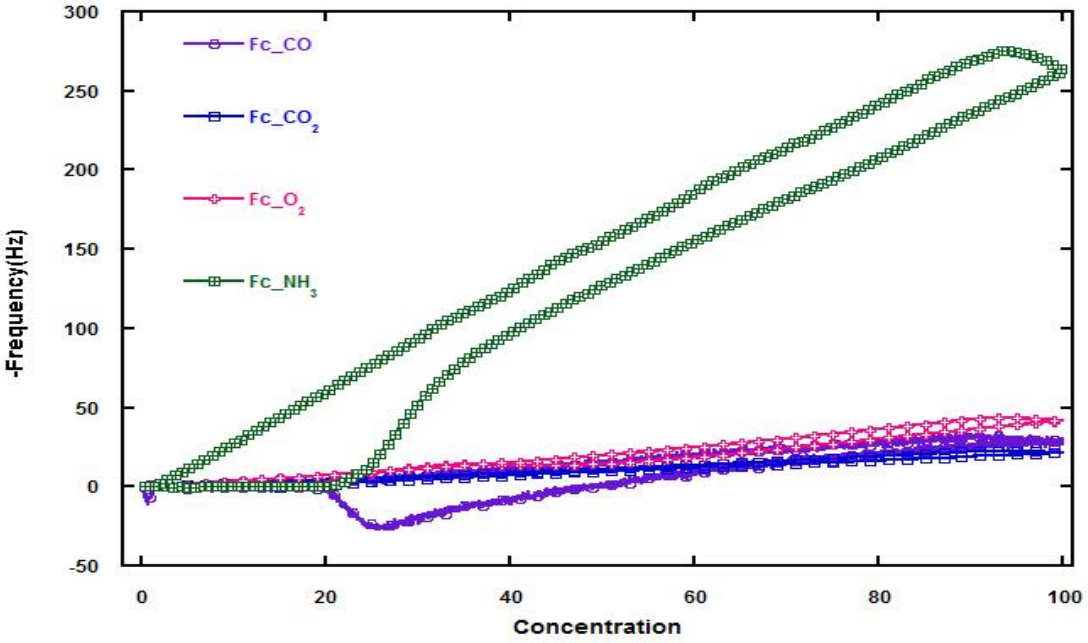

Figure 3.16 : Gas responses of Fc thin-film coatings against CO, CO_2, O_2 and NH_3 under linear gas flow regime.

Figure 3.16 shows gas responses of Fc thin-film coatings against CO, CO_2, O_2 and NH_3 under linear gas flow regime. Response of Fc are mostly linear and have reversible character. For CO gases, non-linear effect is observed.

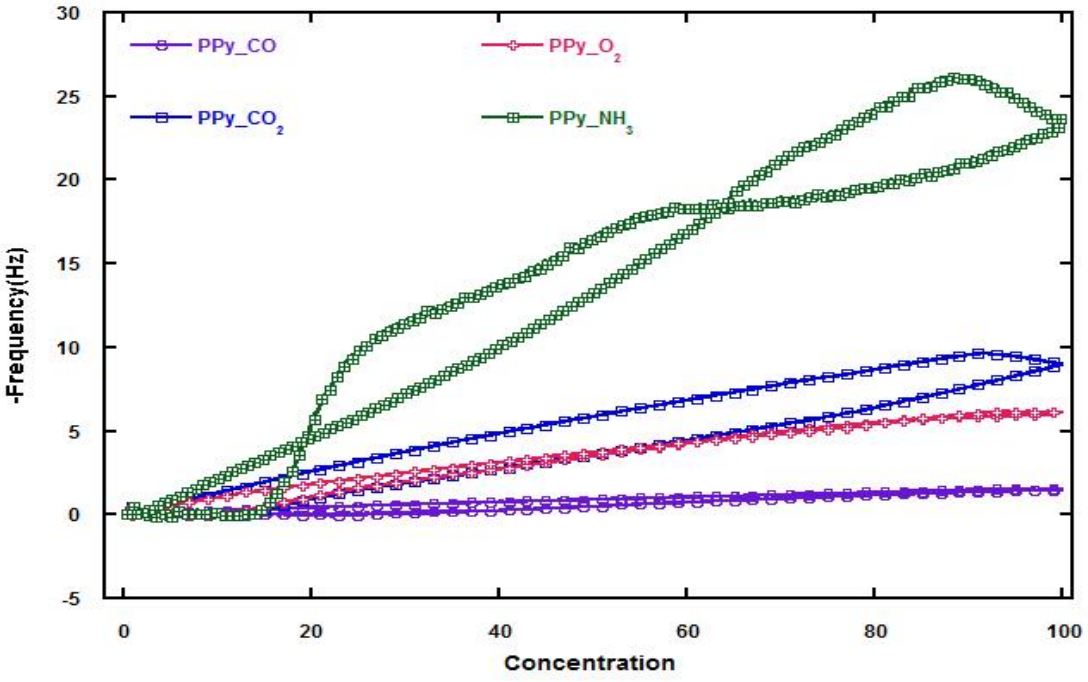

Figure 3.17 : Gas responses of PPy thin-film coatings against CO, CO_2, O_2 and NH_3 under linear gas flow regime.

Figure 3.17 shows gas responses of PPy thin-film coatings against CO, CO_2, O_2 and NH_3 under linear gas flow regime. NH_3 gas showed hysteresis.

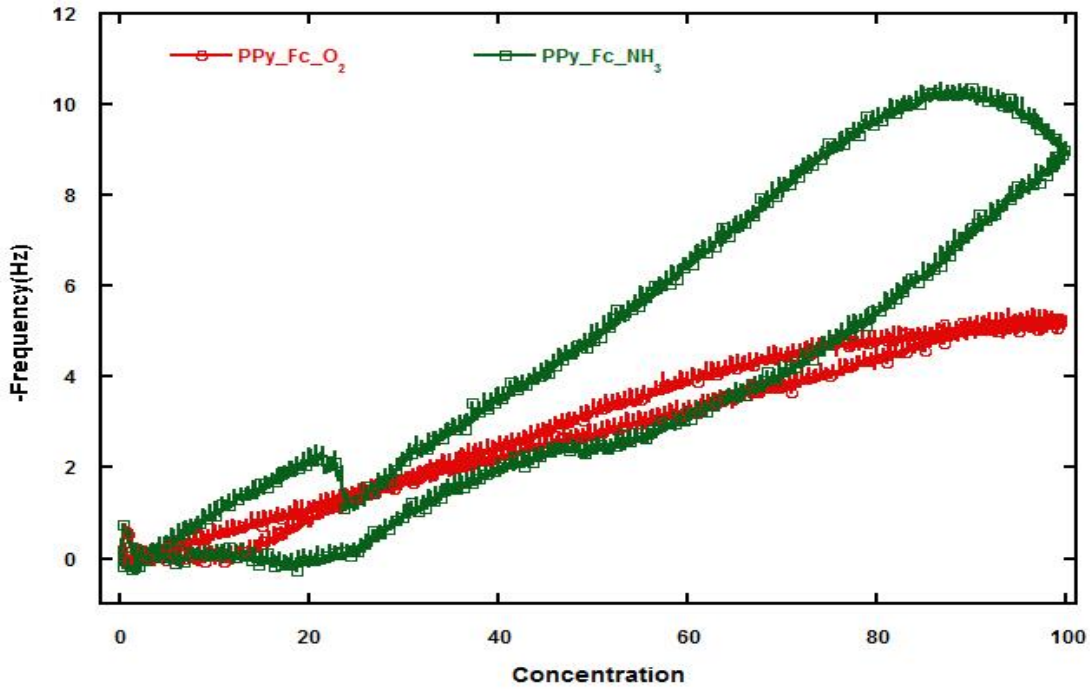

Figure 3.18 : Gas responses of PPy-Fc thin-film coatings against CO, CO_2, O_2 and NH_3 under linear gas flow regime.

Figure 3.18 shows gas responses of PPy-Fc thin-film coatings against CO, CO_2, O_2 and NH_3 under linear gas flow regime. Hysteresis is observed in ammonia result. Meaningful data from CO and CO_2 measurements could not be extracted so they are not located in the graph.

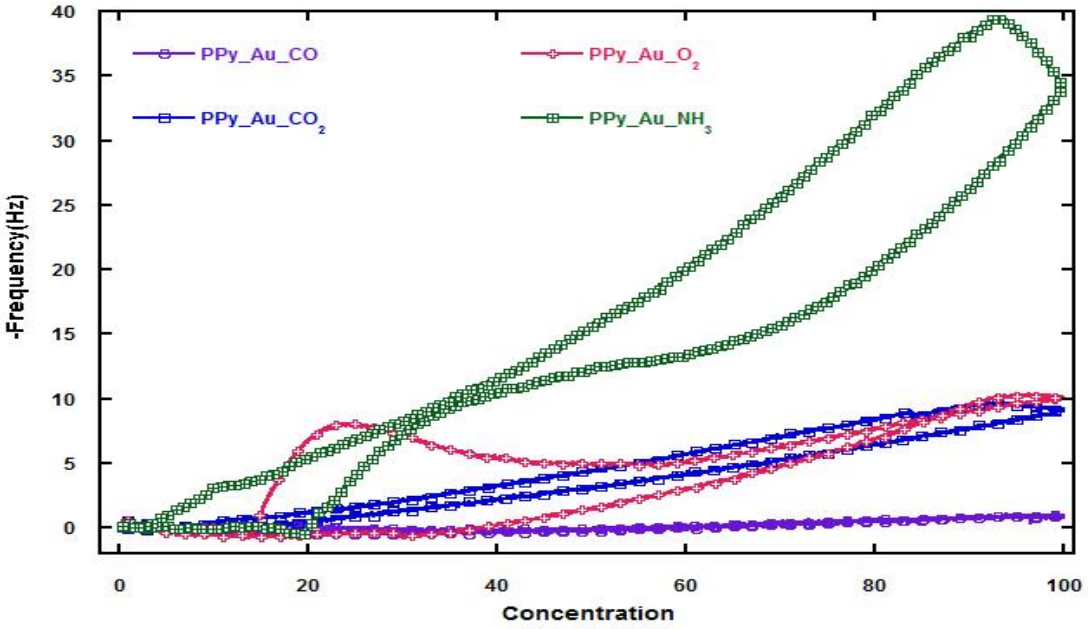

Figure 3.19 : Gas responses of PPy-Au thin-film coatings against CO, CO_2, O_2 and NH_3 under linear gas flow regime.

Figure 3.19 gas responses of PPy-Au thin-film coatings against CO, CO_2, O_2 and NH_3 under linear gas flow regime.

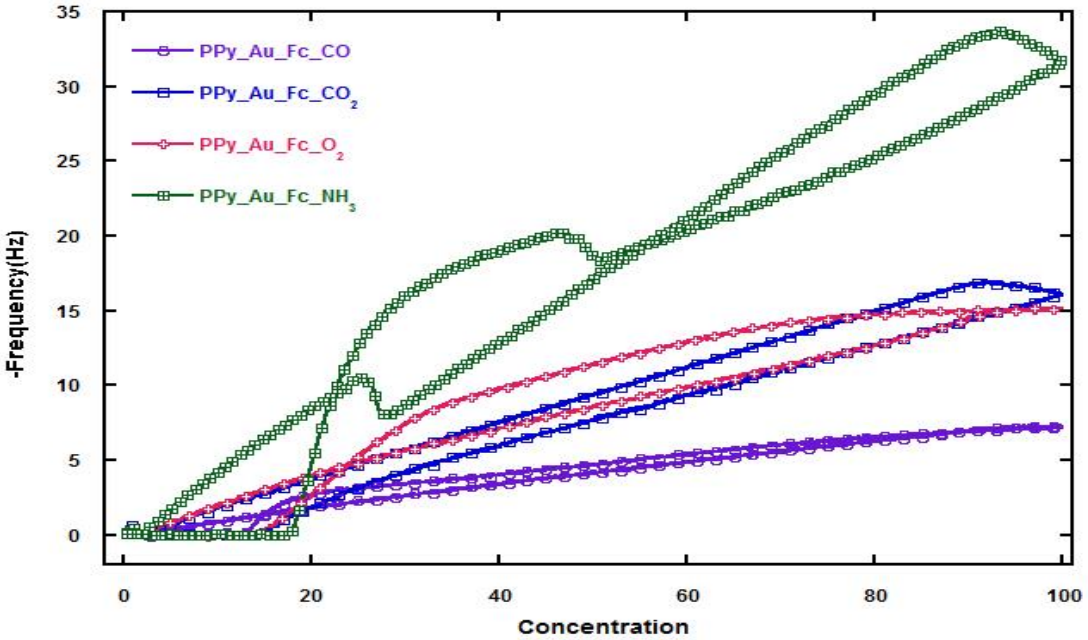

Figure 3.20 : Gas responses of PPy-Au-Fc thin-film coatings against CO, CO_2, O_2 and NH_3 under linear gas flow regime.

Figure 3.20 gas responses of PPy-Au-Fc thin-film coatings against CO, CO_2, O_2 and NH_3 under linear gas flow regime. Hysteresis was observed for NH_3.

3.2. Electrical Results

In this part, IDE electrode measurement results were presented. Variation of resistance of thin-film coating were detected at room temperature. Electrical signal cannot detect for Fc and PPy-Au-Fc despite so much trial.

Thin film swells when exposed to an active gas. Gap between two molecules increases so conductivity decreases. Other reason for the decrease in conductivity is thought to be the physical interaction of active side of coated polimer molecules and unpaired electrons of exposed gas.

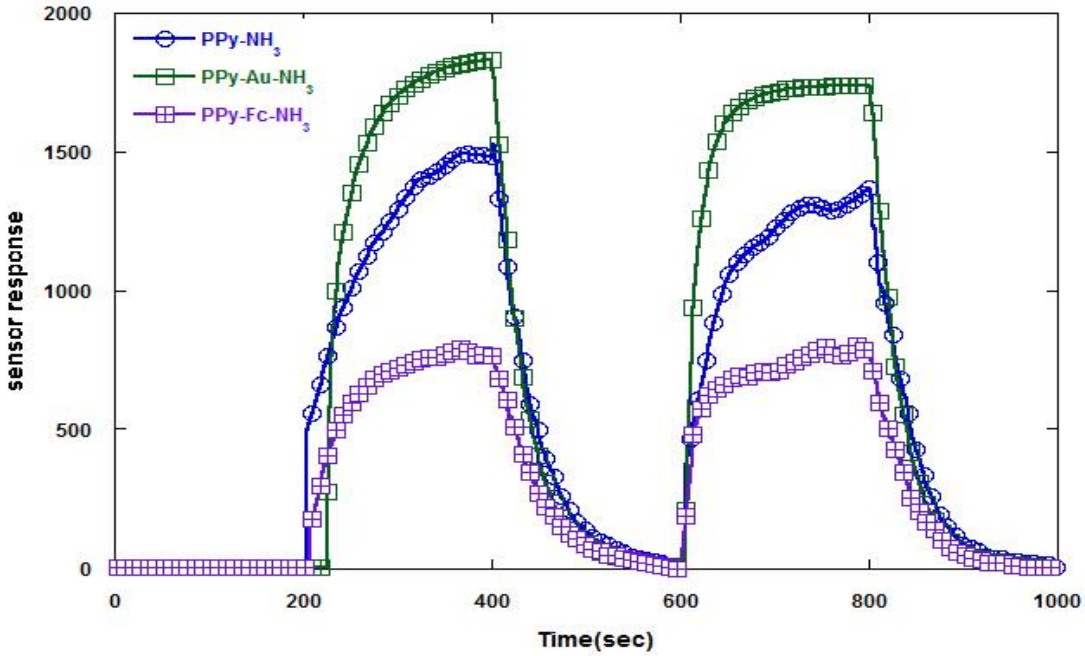

Figure 3.21 : Variation of resistance of thin film coating against NH_3 under periodic gas flow regime.

Electrical response of PPy, PPy-Au and PPy-Fc while exposing to NH_3 is shown at Figure 3.21. Modifiying with ferrocene of PPy decreased the response to ammonia with respect to bare PPy. However, doping with gold nanoparticle of PPy increased sensor response up approximately percentage 1800 and that is the highest sensor response. Thin film behaved reversible.

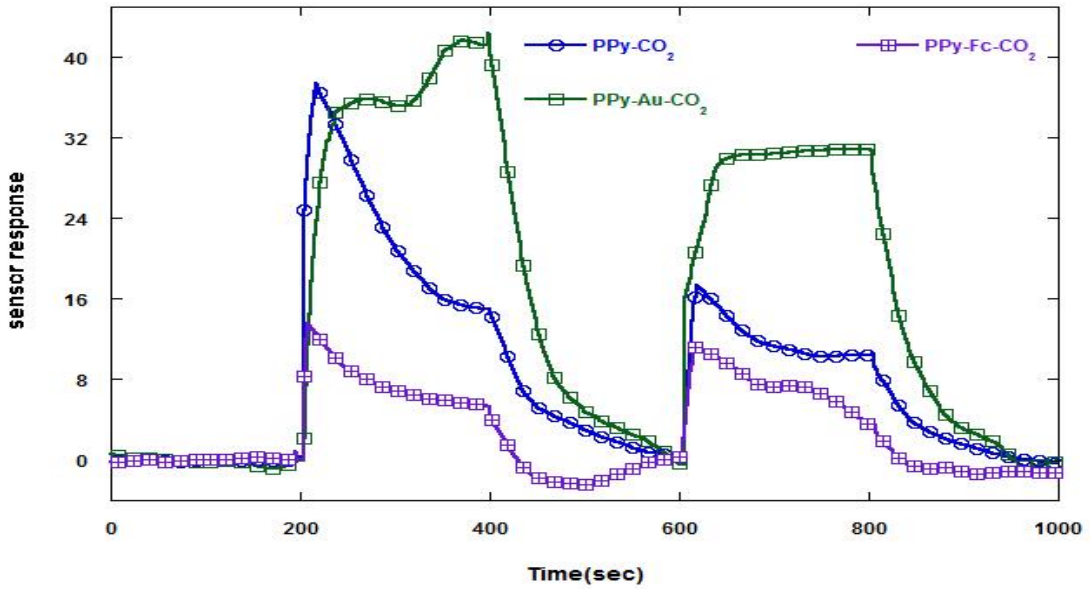

Figure 3.22 : Variation of resistance of thin film coating against CO_2 under periodic gas flow regime.

Resistance variation of thin films against CO_2 is shown in Figure 3.22. Ferrocene modification to PPy decreases the response with respect to bare PPy. However, highest sensor response for CO_2 was observed from the result of gold modification to bare PPy. Neigbour molecules π-orbital is overlap in PPy structure [102]. Along the entire chain of PPy, π-electrons delocalize which cause conducting and semiconducting properties. CO_2 molecules create weak bonds with π-electrons of PPy. That is why resistance increases in the presence of CO_2. The other effect that increases the resistivity of thick film is swelling event. When the film swell, gap between two molecules increases so band gap increases.

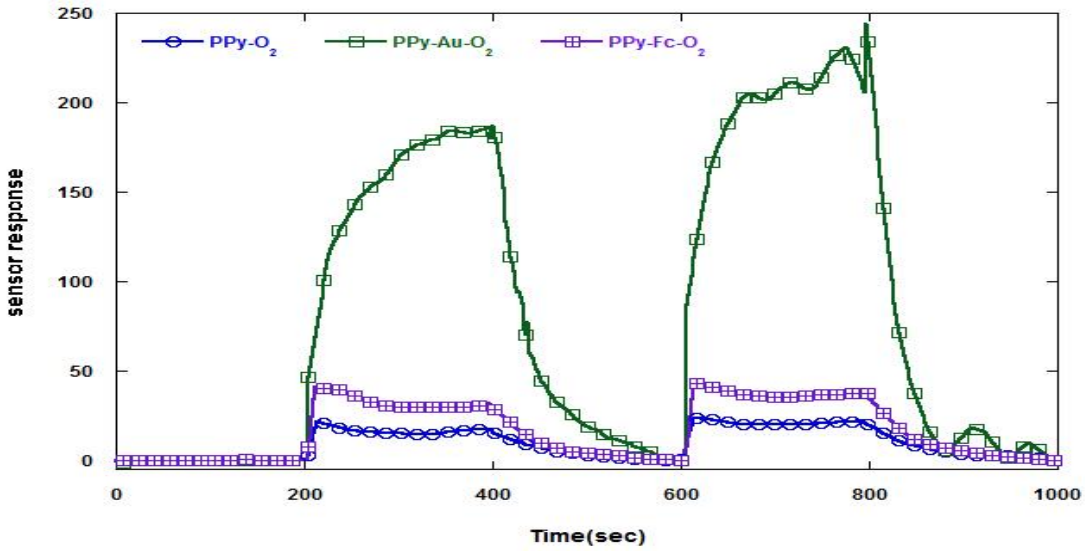

Figure 3.23 : Variation of resistance of thin film coating against O_2 under periodic gas flow regime.

Resistivity response of thin films to O_2 is highest for PPy-Au, while bare PPy and PPy-Fc are close each other and show low sensor response.

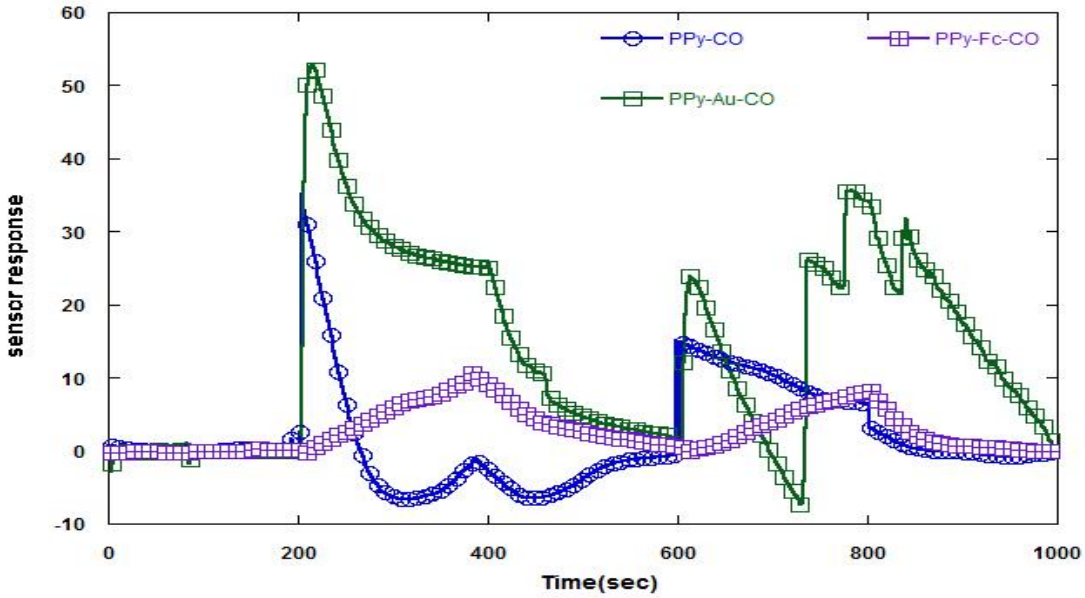

Figure 3.24 : Variation of resistance of thin film coating against CO under periodic gas flow regime.

Figure 3.24 shows sensor response of thin films to CO gas under the periodic gas flow regime. For first cycle of measurements' results are meaningful for both PPy-Au and PPy-Fc. Somehow, at the second cycle of measurements', results are not meaningful for PPy and PPy-Au. Those problems can be thought as some rigidity problem of films, but measurement results of other gases presented above are meaningful and reversible.

4. CONCLUSION

The effect of Au nanoparticle doping on the gas sensing properties of pyrrole-based conductive polymers was investigated via quartz crystal microbalance and interdigitated electrode techniques. Sensor responses of PPy, Fc, PPy-Fc, PPy-Au and PPy-Fc-Au were measured and analyzed against a series of gasses such as CO, CO_2, O_2 and NH_3. For each experiment, parameters such as exposure time and ambient temperature were kept constant.

In the introduction part, some information about gas sensors, conducting polymers, theoretical background, synthesis of materials (done by Mehmet Şenel at Fatih University) and used gases were given. Experimental procedure, gas flow control measurement system and photolithography for IDE fabrication were given in the experimental section. In the last section, QCM and IDE measurement results were given and discussed in details.

The sensor response value of bare PPy was obtained as 5.19 ‰ for CO., but after modification with ferrocene, the sensor response of the PPy-Fc material dropped down to 2.81 ‰. That might be the reason due to molecular structure of PPy-Fc thin film surface with the same number of active sites compare to PPy. After Au doping to PPy-Fc, the sensor response to CO increased back to the same sensor response level of PPy. This might be a result of higher ratio of active surface area and increase in the porousity in the sensing film due to nanoparticle doping. On the other hand, positive QCM behavior, reaching the sensor value of 2.15 ‰, was observed after Au doping of PpyAu. The PPy-Au thin films showed positive QCM response to only CO. The same PPy-Au film was exposed to CO_2, O_2 and NH_3, but negative QCM response was observed, which shows that CO changes viscoelastic properties of the sensing film.

PPy revealed a sensor response value of 8.83 ‰ for CO2, whereas after modification with ferrocene the sensor response of the PPy-Fc material dropped down to 6.80 ‰. This behavior may be a result of low sensor response of Fc to CO2. It should be noted that the same parameters were used, while preparing the thin films of all materials to be able to compare the sensor responses. After Au doping to PPy-Fc, the sensor response against CO_2 increased with respect to PPy-Fc reaching up to 10.33

‰. It can be concluded that Au doping to PPy-Fc increased sensor response against CO_2, whereas Au doping to Ppy decreased sensor response against CO_2 with respect to bare PPy. Modification of Ppy with Fc nearly doubled the sensor response compare to bare Fc, whereas Ppy-Au modification tripled the sensor response to CO_2.

PPy has showed a sensor response value of 28.191 ‰ for NH_3. But, after modification with ferrocene, the sensor response of the Ppy-Fc material rose up to 50.83 ‰, even though bare Fc showed a sensor response value of 36.35. After Au doping to Ppy-Fc, the sensor response to NH_3 decreased compared to Ppy-Fc giving sensor response values close to bare Ppy. On the other handafter Au doping to bare Ppy, the sensor response to NH_3 dropped to the half Finally, PPy showed a sensor response value of 5.60 ‰ for O_2, whereas ferrocene showed a sensor response value of 15.11 ‰. The surface properties of the films might be different due solubility properties of the materials in DMF, since Fc is soluble in DMF but PPy is insoluble. This might effect the film qualities of the materials. After modification of PPy with Fc and subsequent Au doping, the sensor response to O_2 was increased to 12.7 ‰ with respect to Fc. Increasing on response of PPy-Fc-Au might be related with additional ferrocene active sites and increase surface area in the modified film.

All the materials, e.g. Ppy, Ppy-Au, Fc, Ppy-Fc, have showed selective behaviors specifically to NH3. The electrical IDE sensor signals could only have been obtained with IDE measurements for PPy, PPy-Au and PPy-Fc materials. We have observed that the sensitivity of Au-doped PPy has been increased with respect to bare PPy for all types of gases. On the contrary, the modification of PPy with Fc decreased the sensitivity with respect to the bare PPy for all types of gases. Metal doping are used to increase the conductivity of the conducting polymer composite material [5-7].

As a conclusion, the experimental results obtained in this study showed varying degrees of sensor responses, making them easy to use as practical ammonia sensors due to the high sensitive behaviors of the investigated materials. Au-doped PPy, increasing selectivity against O_2, has not been studied as gas sensor in literature so far. Future studies may focus on functionalization of PPy with different molecules to increase selectivity properties of conducting polymers against an other specific gas molecule.

5. REFERENCES

1. **Yamazoe, N.**, (2005). *Toward innovations of gas sensor technology*. Sensors and Actuators B: Chemical, **108**(1): p. 2-14.
2. **Taylor, R.F. and J.S. Schultz**, (2010). *Handbook of chemical and biological sensors*. CRC Press.
3. **Fine, G.F., et al.**, (2010). *Metal oxide semi-conductor gas sensors in environmental monitoring.* Sensors, **10**(6): p. 5469-5502.
4. **Yamazoe, N.**, (2005). *Toward innovations of gas sensor technology*. Sensors and Actuators B: Chemical, **108**(1–2): p. 2-14.
5. **Ram, M.K., et al.**, (2005). *CO gas sensing from ultrathin nano-composite conducting polymer film.* Sensors and Actuators B: Chemical, **106**(2): p. 750-757.
6. **Ando, M., T. Kobayashi, and M. Haruta**, (1997). *Combined effects of small gold particles on the optical gas sensing by transition metal oxide films.* Catalysis Today, **36**(1): p. 135-141.
7. **Ando, M., R. Chabicovsky, and M. Haruta**, (2001). *Optical hydrogen sensitivity of noble metal–tungsten oxide composite films prepared by sputtering deposition.* Sensors and Actuators B: Chemical, **76**(1): p. 13-17.
8. **Di Natale, C., et al.**, (1998). *Characterization and design of porphyrins-based broad selectivity chemical sensors for electronic nose applications.* Sensors and Actuators B: Chemical, **52**(1): p. 162-168.
9. **Zhu, C., et al.**, (2006). *A precise sensor for SF 6 based on piezoelectric ultrasound.* Xiyou Jinshu Cailiao yu Gongcheng(Rare Metal Materials and Engineering), **35**: p. 157-158.
10. **Yamamoto, O., T. Takuma, and M. Kinouchi**, (2002). *Recovery of SF/sub 6/from N/sub 2//SF/sub 6/gas mixtures by using a polymer membrane.* Electrical Insulation Magazine, IEEE, **18**(3): p. 32-37.
11. **Wongchoosuk, C., et al.**, (2010). *Multi-walled carbon nanotube-doped tungsten oxide thin films for hydrogen gas sensing.* Sensors, **10**(8): p. 7705-7715.
12. **Wang, Y., et al.**, (2010). *Improving the performance of catalytic combustion type methane gas sensors using nanostructure elements doped with rare earth cocatalysts.* Sensors, **11**(1): p. 19-31.
13. **Vashpanov, Y., H. Choo, and D.S. Kim**, (2011). *Dynamic control of adsorption sensitivity for photo-EMF-based ammonia gas sensors using a wireless network.* Sensors, **11**(11): p. 10930-10939.
14. **Tong, L., et al.** (2004). *Oil-gas separation mechanism of polymer membranes applied to online transformer dissolved gases monitoring*. in *Electrical Insulation, 2004. Conference Record of the 2004 IEEE International Symposium on*. IEEE.
15. **Minglei, S., et al.** (2010). *Gas concentration detection using ultrasonic based on wireless sensor networks*. in *Information Science and Engineering (ICISE), 2010 2nd International Conference on*. IEEE.

16. **Manzoli, A., et al.**, (2011). *Low-cost gas sensors produced by the graphite line-patterning technique applied to monitoring banana ripeness.* Sensors, **11**(6): p. 6425-6434.
17. **Liu, J., et al.**, (2011). *Advances in SAW gas sensors based on the condensate-adsorption effect.* Sensors, **11**(12): p. 11871-11884.
18. **Kulinyi, S., et al.**, (2005). *Olfactory detection of methane, propane, butane and hexane using conventional transmitter norms.* Sensors and Actuators B: Chemical, **111**: p. 286-292.
19. **Huyen, D.N., et al.**, (2011). *Effect of TiO2 on the gas sensing features of TiO2/PANi nanocomposites.* Sensors, **11**(2): p. 1924-1931.
20. **Duval, M.**, (2003). *New techniques for dissolved gas-in-oil analysis.* Electrical insulation magazine, IEEE, **19**(2): p. 6-15.
21. **Ding, W., et al.**, (2006). *Calibration methods of carbon nanotube gas sensor for partial discharge detection in SF/sub 6.* Dielectrics and Electrical Insulation, IEEE Transactions on, **13**(2): p. 353-361.
22. **Chinvongamorn, C., et al.**, (2008). *Amperometric determination of sulfite by gas diffusion-sequential injection with boron-doped diamond electrode.* Sensors, **8**(3): p. 1846-1857.
23. **Chen, D., S. Lei, and Y. Chen**, (2011). *A single polyaniline nanofiber field effect transistor and its gas sensing mechanisms.* Sensors, **11**(7): p. 6509-6516.
24. **Changping, Z., et al.**, (2005). *Microconcentration detector for SF6 based on CPLD.* Chinese Journal of Scientific Instrument, **26**(8): p. 448-449.
25. **Chang, Y.-C., et al.**, (2011). *Bromocresol green/mesoporous silica adsorbent for ammonia gas sensing via an optical sensing instrument.* Sensors, **11**(4): p. 4060-4072.
26. **Catalan, L.J., V. Liang, and C.Q. Jia**, (2006). *Comparison of various detection limit estimates for volatile sulphur compounds by gas chromatography with pulsed flame photometric detection.* Journal of chromatography A, **1136**(1): p. 89-98.
27. **Anderson, T., et al.**, (2009). *Advances in hydrogen, carbon dioxide, and hydrocarbon gas sensor technology using GaN and ZnO-based devices.* Sensors, **9**(6): p. 4669-4694.
28. **Tardy, P., et al.**, (2004). *Dynamic thermal conductivity sensor for gas detection.* Sensors and Actuators B: Chemical, **98**(1): p. 63-68.
29. **Sonoyama, M., Y. Kato, and H. Fujita**. (2010). *Application of ultrasonic to a hydrogen sensor*. in *Sensors, 2010 IEEE*. IEEE.
30. **Miya, H., et al.** (2009). *Compact Raman Lidar for hydrogen gas leak detection*. in *Conference on Lasers and Electro-Optics/Pacific Rim*. Optical Society of America.
31. **Marr, I., et al.**, (2011). *Planar zeolite film-based potentiometric gas sensors manufactured by a combined thick-film and electroplating technique.* Sensors, **11**(8): p. 7736-7748.
32. **Koplin, T.J., et al.**, (2006). *Workflow for high throughput screening of gas sensing materials.* Sensors, **6**(4): p. 298-307.
33. **Iannotta, S., et al.** (2008). *Novel Nano-Hybrid gas sensor based on n-TiO2 functionalized by phthalocyanines via supersonic beam co-deposition: performance and application to automotive air quality*. in *Sensors, 2008 IEEE*. IEEE.

34. **Ho, K.-C., W.-T. Hung, and J.-C. Yang**, (2003). *On the Electrooxidation and amperometric detection of no gas at the pt/nafion® electrode.* Sensors, **3**(8): p. 290-303.
35. **Haiming, Z.** (2008). *Experiment Study of continuous emission monitoring system based on Differential Optical Absorption Spectroscopy*. in *Education Technology and Training, 2008. and 2008 International Workshop on Geoscience and Remote Sensing. ETT and GRS 2008. International Workshop on*. IEEE.
36. **Frodl, R. and T. Tille**, (2006). *A high-precision NDIR gas sensor for automotive applications.* IEEE Sensors Journal, **6**(6).
37. **Fleming, W.J.**, (2001). *Overview of automotive sensors.* Sensors Journal, IEEE, **1**(4): p. 296-308.
38. **Endres, H.-E., et al.**, (1996). *A thin-film SnO< sub> 2</sub> sensor system for simultaneous detection of CO and NO< sub> 2</sub> with neural signal evaluation.* Sensors and Actuators B: Chemical, **36**(1): p. 353-357.
39. **Caucheteur, C., et al.**, (2008). *Catalytic fiber Bragg grating sensor for hydrogen leak detection in air.* Photonics Technology Letters, IEEE, **20**(2): p. 96-98.
40. **Billi, E., et al.**, (2002). *Development of a protected gas sensor for exhaust automotive applications.* Sensors Journal, IEEE, **2**(4): p. 342-348.
41. **Belov, I., et al.** (2004). *Thermal and flow analysis of SiC-based gas sensors for automotive applications*. in *Thermal and Mechanical Simulation and Experiments in Microelectronics and Microsystems, 2004. EuroSimE 2004. Proceedings of the 5th International Conference on*. IEEE.
42. **Tamaekong, N., et al.**, (2010). *Flame-spray-made undoped zinc oxide films for gas sensing applications.* Sensors, **10**(8): p. 7863-7873.
43. **Yi, W., et al.** (2009). *Measurement of CH4 by differential infrared optical absorption spectroscopy*. in *Electronic Measurement & Instruments, 2009. ICEMI'09. 9th International Conference on*. IEEE.
44. **Xiao, G., et al.** (2011). *Trace amount formaldehyde gas detection for indoor air quality monitoring*. in *Instrumentation and Measurement Technology Conference (I2MTC), 2011 IEEE*. IEEE.
45. **Kim, S.-J., et al.**, (2011). *Design of selective gas sensors using additive-loaded In2O3 hollow spheres prepared by combinatorial hydrothermal reactions.* Sensors, **11**(11): p. 10603-10614.
46. **Kim, K.-S., et al.**, (2010). *A nanopore structured high performance toluene gas sensor made by nanoimprinting method.* Sensors, **10**(1): p. 765-774.
47. **Ke, M.-T., et al.**, (2009). *A MEMS-based benzene gas sensor with a self-heating wo3 sensing layer.* Sensors, **9**(4): p. 2895-2906.
48. **Johan, S., et al.** (2007). *Remote moisture sensing utilizing ordinary RFID tags*. in *Sensors, 2007 IEEE*. IEEE.
49. **Fraiwan, L., et al.** (2011). *A wireless home safety gas leakage detection system*. in *Biomedical Engineering (MECBME), 2011 1st Middle East Conference on*. IEEE.
50. **Emadi, T.A., et al.** (2009). *Development of a polymer-based gas sensor-humidity and CO< inf> 2</inf> sensitivity*. in *Microsystems and Nanoelectronics Research Conference, 2009. MNRC 2009. 2nd*. IET.
51. **Ding, B., et al.**, (2009). *Gas sensors based on electrospun nanofibers.* Sensors, **9**(3): p. 1609-1624.
52. **Cubillas, A.M., et al.**, (2009). *Gas sensor based on photonic crystal fibres in the 2v3 and v2+ 2v3 vibrational bands of methane.* Sensors, **9**(8): p. 6261-6272.

53. **Chou, S.M., et al.**, (2006). *ZnO: Al thin film gas sensor for detection of ethanol vapor.* Sensors, **6**(10): p. 1420-1427.
54. **Bakrania, S.D. and M.S. Wooldridge**, (2010). *The effects of the location of Au additives on combustion-generated SnO2 nanopowders for co gas sensing.* Sensors, **10**(7): p. 7002-7017.
55. **Yamazoe, N. and K. Shimanoe**, (2008). *Theory of power laws for semiconductor gas sensors.* Sensors and Actuators B: Chemical, **128**(2): p. 566-573.
56. **Kanan, S.M., et al.**, (2009). *Semiconducting metal oxide based sensors for selective gas pollutant detection.* Sensors, **9**(10): p. 8158-8196.
57. **Wang, C., et al.**, (2010). *Metal oxide gas sensors: sensitivity and influencing factors.* Sensors, **10**(3): p. 2088-2106.
58. **Yeung, C.S., Y.K. Chen, and Y.A. Wang**, (2011). *Defected and Substitutionally Doped Nanotubes: Applications in Biosystems, Sensors, Nanoelectronics, and Catalysis.*
59. **Richardson, T., et al.**, (2006). *The NO< sub> 2</sub> gas sensing properties of calixarene/porphyrin mixed LB films.* Colloids and Surfaces A: Physicochemical and Engineering Aspects, **284**: p. 320-325.
60. **Chou, J.**, (2000). *Hazardous gas monitors: a practical guide to selection, operation and applications*. McGraw-Hill Professional.
61. **Albert, K.J., et al.**, (2000). *Cross-reactive chemical sensor arrays.* Chemical Reviews, **100**(7): p. 2595-2626.
62. **Chiang, C.K., et al.**, (1977). *Electrical Conductivity in Doped Polyacetylene.* Physical Review Letters, **39**(17): p. 1098-1101.
63. **Greenham, N.C., et al.**, (1993). *Efficient light-emitting diodes based on polymers with high electron affinities.* Nature, **365**(6447): p. 628-630.
64. **Friend, R., et al.**, (1999). *Electroluminescence in conjugated polymers.* Nature, **397**(6715): p. 121-128.
65. **List, E.J.W., et al.**, (2002). *The Effect of Keto Defect Sites on the Emission Properties of Polyfluorene-Type Materials.* Advanced Materials, **14**(5): p. 374-378.
66. **Schmidt-Mende, L., et al.**, (2001). *Self-Organized Discotic Liquid Crystals for High-Efficiency Organic Photovoltaics.* Science, **293**(5532): p. 1119-1122.
67. **Liscio, A., et al.**, (2007). *Photovoltaic Charge Generation Visualized at the Nanoscale: A Proof of Principle.* Journal of the American Chemical Society, **130**(3): p. 780-781.
68. **Thompson, B.C. and J.M.J. Fréchet**, (2008). *Polymer–Fullerene Composite Solar Cells.* Angewandte Chemie International Edition, **47**(1): p. 58-77.
69. **Dance, Z.E.X., et al.**, (2008). *Direct Observation of the Preference of Hole Transfer over Electron Transfer for Radical Ion Pair Recombination in Donor−Bridge−Acceptor Molecules.* Journal of the American Chemical Society, **130**(3): p. 830-832.
70. **Hagberg, D.P., et al.**, (2008). *Molecular Engineering of Organic Sensitizers for Dye-Sensitized Solar Cell Applications.* Journal of the American Chemical Society, **130**(19): p. 6259-6266.
71. **Muccini, M.**, (2006). *A bright future for organic field-effect transistors.* Nat Mater, **5**(8): p. 605-13.
72. **Gao, P., et al.**, (2008). *Benzo[1,2-b:4,5-b']bis[b]benzothiophene as solution processible organic semiconductor for field-effect transistors.* Chemical Communications, (13).

73. **Usta, H., A. Facchetti, and T.J. Marks**, (2008). *Air-stable, solution-processable n-channel and ambipolar semiconductors for thin-film transistors based on the indenofluorenebis (dicyanovinylene) core.* Journal of the American Chemical Society, **130**(27): p. 8580-8581.
74. **Yang, C., et al.**, (2008). *Functionalized Methanofullerenes Used as n-Type Materials in Bulk-Heterojunction Polymer Solar Cells and in Field-Effect Transistors.* Journal of the American Chemical Society, **130**(20): p. 6444-6450.
75. **Palma, M., et al.**, (2006). *Self-Organization and Nanoscale Electronic Properties of Azatriphenylene-Based Architectures: A Scanning Probe Microscopy Study.* Advanced Materials, **18**(24): p. 3313-3317.
76. **Chen, X., et al.**, (2008). *On-Wire Lithography-Generated Molecule-Based Transport Junctions: A New Testbed for Molecular Electronics.* Journal of the American Chemical Society, **130**(26): p. 8166-8168.
77. **Choi, T.-L., et al.**, (2007). *Synthesis and Nonvolatile Memory Behavior of Redox-Active Conjugated Polymer-Containing Ferrocene.* Journal of the American Chemical Society, **129**(32): p. 9842-9843.
78. **Schwendeman, I., et al.**, (2002). *Enhanced Contrast Dual Polymer Electrochromic Devices.* Chemistry of Materials, **14**(7): p. 3118-3122.
79. **Meng, H., et al.**, (2003). *An Unusual Electrochromic Device Based on a New Low-Bandgap Conjugated Polymer.* Advanced Materials, **15**(2): p. 146-149.
80. **Bange, K. and T. Gambke**, (1990). *Electrochromic Materials for optical switching devices.* Advanced Materials, **2**(1): p. 10-16.
81. **Pennisi, A., et al.**, (1999). *Preliminary test of a large electrochromic window.* Electrochimica Acta, **44**(18): p. 3237-3243.
82. **Rauh, R.D.**, (1999). *Electrochromic windows: an overview.* Electrochimica Acta, **44**(18): p. 3165-3176.
83. **Rosseinsky, D.R. and R.J. Mortimer**, (2001). *Electrochromic Systems and the Prospects for Devices.* Advanced Materials, **13**(11): p. 783-793.
84. **Lu, X., et al.**, (2011). *One-dimensional conducting polymer nanocomposites: Synthesis, properties and applications.* Progress in Polymer Science, **36**(5): p. 671-712.
85. **Lippmann, M.**, (1881). *On the principle of the conservation of electricity.*
86. **Sauerbrey, G.**, (1959). *Verwendung von Schwingquarzen zur Wägung dünner Schichten und zur Mikrowägung.* Zeitschrift für Physik, **155**(2): p. 206-222.
87. **Buck, R.P., et al.**, (2004). *Piezoelectric chemical sensors - (IUPAC Technical Report).* Pure and Applied Chemistry, **76**(6): p. 1139-1160.
88. **Janshoff, A., H.J. Galla, and C. Steinem**, (2000). *Piezoelectric mass-sensing devices as biosensors - An alternative to optical biosensors?* Angewandte Chemie-International Edition, **39**(22): p. 4004-4032.
89. **Sauerbrey, G.**, (1959). *Use of quartz vibration for weighing thin films on a microbalance.* J. Physik, **155**: p. 206-212.
90. **Janata, J.**, (2009). *Principles of chemical sensors*. Springer.
91. **Bottom, V.E.**, (1982). *Introduction to quartz crystal unit design*. Van Nostrand Reinhold New York.
92. **Johannsmann, D.**, (2001). *Derivation of the shear compliance of thin films on quartz resonators from comparison of the frequency shifts on different harmonics: A perturbation analysis.* Journal of Applied Physics, **89**(11): p. 6356-6364.

93. **Gomes, M., P.S.T. Nogueira, and J.A. Oliveira**, (2000). *Quantification of CO< sub> 2</sub>, SO< sub> 2</sub>, NH< sub> 3</sub>, and H< sub> 2</sub> S with a single coated piezoelectric quartz crystal.* Sensors and Actuators B: Chemical, **68**(1): p. 218-222.
94. **Glassford, A.**, (1978). *Response of a quartz crystal microbalance to a liquid deposit.* Journal of Vacuum Science and Technology, **15**(6): p. 1836-1843.
95. **Lee, S.-H., et al.**, (2005). *Rapid detection of bacterial spores using a quartz crystal microbalance (QCM) immunoassay.* Sensors Journal, IEEE, **5**(4): p. 737-743.
96. **Hunt, W.D., D.D. Stubbs, and S.-H. Lee**, (2003). *Time-dependent signatures of acoustic wave biosensors*. Proceedings of the IEEE, **91**(6): p. 890-901.
97. **Corso, C.D., et al.**, (2006). *Real-time detection of mesothelin in pancreatic cancer cell line supernatant using an acoustic wave immunosensor.* Cancer Detection and Prevention, **30**(2): p. 180-187.
98. **Lalauze, R.**, (2010). *Adsorption Phenomena*, in *Physical Chemistry of Solid-Gas Interfaces*. 2010, ISTE. p. 1-27.
99. **Şenel, M.**, (2011). *Construction of reagentless glucose biosensor based on ferrocene conjugated polypyrrole.* Synthetic Metals, **161**(17–18): p. 1861-1868.
100. **Bai, H. and G. Shi**, (2007). *Gas Sensors Based on Conducting Polymers.* Sensors, **7**(3): p. 267-307.
101. **Ullah, H., et al.**, (2013). *Theoretical insight of polypyrrole ammonia gas sensor.* Synthetic Metals, **172**: p. 14-20.
102. **Waghuley, S., et al.**, (2008). *Application of chemically synthesized conducting polymer-polypyrrole as a carbon dioxide gas sensor.* Sensors and Actuators B: Chemical, **128**(2): p. 366-373.